

# Tectonics

## RESEARCH ARTICLE

10.1029/2021TC006751

### Key Points:

- A new *ca.* 1,780 Ma paleomagnetic pole reconstructs the Superior province of Laurentia to moderately high latitudes
- This pole establishes the coherency of the Laurentia craton following Trans-Hudson orogenesis and supports the northern Europe and North America connection with Baltica
- Paleomagnetic and geologic data from Laurentia strongly support mobile-lid plate tectonics from 2.2 Ga to the present day

### Supporting Information:

Supporting Information may be found in the online version of this article.

### Correspondence to:

N. L. Swanson-Hysell,  
[swanson-hysell@berkeley.edu](mailto:swanson-hysell@berkeley.edu)

### Citation:

Swanson-Hysell, N. L., Avery, M. S., Zhang, Y., Hodgin, E. B., Sherwood, R. J., Apen, F. E., et al. (2021). The paleogeography of Laurentia in its early years: New constraints from the Paleoproterozoic East-Central Minnesota Batholith. *Tectonics*, *40*, e2021TC006751. <https://doi.org/10.1029/2021TC006751>

Received 1 FEB 2021

Accepted 8 APR 2021

# The Paleogeography of Laurentia in Its Early Years: New Constraints From the Paleoproterozoic East-Central Minnesota Batholith

Nicholas L. Swanson-Hysell<sup>1</sup> , Margaret S. Avery<sup>1</sup> , Yiming Zhang<sup>1</sup>, Eben B. Hodgin<sup>1</sup>, Robert J. Sherwood<sup>1</sup>, Francisco E. Apen<sup>2</sup> , Terrence J. Boerboom<sup>3</sup>, C. Brenhin Keller<sup>1,4,5</sup>, and John M. Cottle<sup>2</sup>

<sup>1</sup>Department of Earth and Planetary Science, University of California Berkeley, Berkeley, CA, USA, <sup>2</sup>Department of Earth Science, University of California Santa Barbara, Santa Barbara, CA, USA, <sup>3</sup>Minnesota Geological Survey, Saint Paul, MN, USA, <sup>4</sup>Berkeley Geochronology Center, Berkeley, CA, USA, <sup>5</sup>Department of Earth Sciences, Dartmouth College, Hanover, NH, USA

**Abstract** The *ca.* 1.83 Ga Trans-Hudson orogeny resulted from collision of an upper plate consisting of the Hearne, Rae, and Slave provinces with a lower plate consisting of the Superior province. While the geologic record of *ca.* 1.83 Ga peak metamorphism within the orogen suggests that these provinces were a single amalgamated craton from this time onward, a lack of paleomagnetic poles from the Superior province following Trans-Hudson orogenesis has made this coherency difficult to test. We develop a high-quality paleomagnetic pole for northeast-trending diabase dikes of the post-Penokean orogen East-Central Minnesota Batholith (pole longitude: 265.8°; pole latitude: 20.4°;  $A_{95}$ : 4.5°; K: 45.6 N: 23) whose age we constrain to be  $1,779.1 \pm 2.3$  Ma (95% CI) with new U-Pb dates. Demagnetization and low-temperature magnetometry experiments establish dike remanence be held by low-Ti titanomagnetite. Thermochronology data constrain the intrusions to have cooled below magnetite blocking temperatures upon initial emplacement with a mild subsequent thermal history within the stable craton. The similarity of this new Superior province pole with poles from the Slave and Rae provinces establishes the coherency of Laurentia following Trans-Hudson orogenesis. This consistency supports interpretations that older discrepant 2.22–1.87 Ga pole positions between the provinces are the result of differential motion through mobile-lid plate tectonics. The new pole supports the northern Europe and North America connection between the Laurentia and Fennoscandia cratons. The pole can be used to jointly reconstruct these cratons *ca.* 1,780 Ma strengthening the paleogeographic position of these major constituents of the hypothesized late Paleoproterozoic supercontinent Nuna.

**Plain Language Summary** North America is a really old continent. Geologists refer to the ancient interior of North America as Laurentia. Laurentia first formed around 1.8 billion years ago when microcontinents collided into each other forming the Trans-Hudson mountain belt. We know that continents move through time and that Laurentia must have been in a different place. We can determine the ancient position by using the magnetism of rocks formed from cooling magma. Magnetic minerals in rocks act like frozen compass needles that tell us which way was north for the continent and how close it was to the equator. In this research, we developed magnetic data from rocks that formed 1.78 billion years ago in Minnesota, USA. We were able to determine how old the rocks are by measuring the uranium in minerals. We can compare this magnetic direction to rocks of the same age from far on the other side of Laurentia (in Arctic Canada). This comparison confirms that the regions were together following the Trans-Hudson mountain building (and that they were joined with a big piece of northern Europe). Magnetic directions from older rocks are distinct between the microcontinents as they traveled separately through plate tectonics prior to their collision.

## 1. Introduction

In the Orosirian Period of the Paleoproterozoic Era, a series of collisional orogenies led to the amalgamation of Archean provinces to form the core of the Laurentia craton (Figure 1; Hoffman, 1988; Whitmeyer & Karlstrom, 2007). The most significant of these orogenies was the *ca.* 1,850–1,800 Ma Trans-Hudson

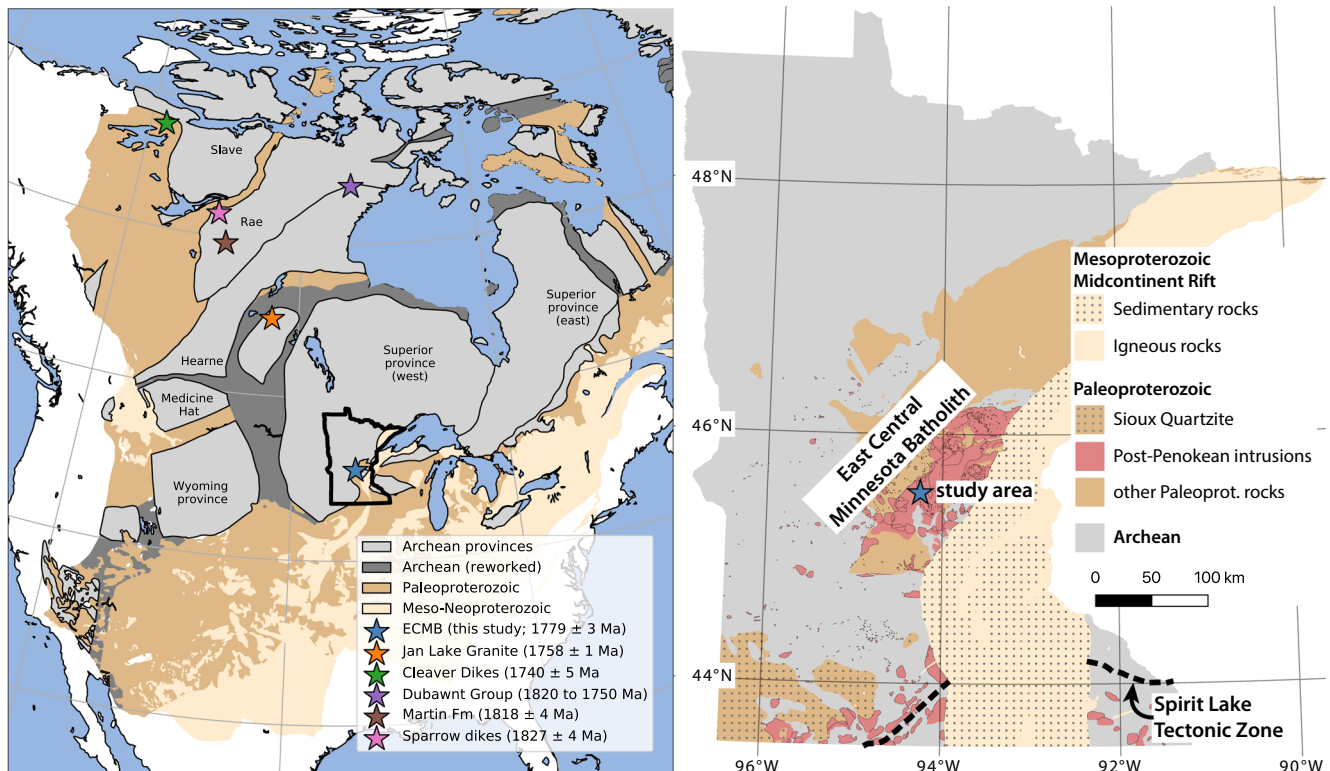


**Figure 1.** Map of Laurentia showing the location of Archean provinces and younger Proterozoic crust (simplified from Whitmeyer & Karlstrom, 2007). The localities of paleomagnetic poles that constrain Laurentia’s position just after its amalgamation are shown with stars including the new pole from this study developed from the East-Central Minnesota Batholith (ECMB). The outline of the state of Minnesota around the ECMB blue star is the region for the geologic map in the right panel. This map shows interpreted Precambrian geology for the state of Minnesota (simplified from Jirsa et al., 2012) including in regions covered by Phanerozoic sedimentary rocks where the Precambrian bedrock is inferred from geophysical data and drill cores.

orogeny associated with the collision between the Superior province and the Churchill province which comprised a composite of the Slave, Hearne and Rae provinces (Figure 1; Weller & St-Onge, 2017). The length of the orogen as well as the pressure-temperature of metamorphism within it are similar to that of continent-continent collision within the Himalayan orogen (Weller & St-Onge, 2017). The terminal closure of the intervening ocean basin between the Superior and composite Slave + Hearne + Rae provinces is interpreted in paleogeographic models to be associated not only with the assembly of Laurentia, but also with the conjoining of other continents into the hypothesized supercontinent Nuna (Pehrsson et al., 2015).

The rapid Paleoproterozoic amalgamation of the Laurentia craton led to the large persistent area of continental lithosphere that would grow further through accretionary orogenesis subsequently in the Paleoproterozoic Era and through the Mesoproterozoic Era (Whitmeyer & Karlstrom, 2007). This subsequent orogenesis along the southern to eastern margin of Laurentia (present-day coordinates) indicates that it was a long-lived accretionary margin (Karlstrom et al., 2001; Whitmeyer & Karlstrom, 2007). This accretionary margin has been interpreted to have extended beyond Laurentia and have continued onto Baltica and Australia (Karlstrom et al., 2001). Based on correlation of Archean provinces and Paleoproterozoic orogenic belts, Gower et al. (1990) reconstructed Baltica to Laurentia in a position known as the NENA (northern Europe and North America) configuration. This reconstruction is compatible with existing paleomagnetic constraints from ca. 1,750 to 1,270 Ma (Evans & Pisarevsky, 2008) and these conjoined cratons feature as a major component of the hypothesized Nuna supercontinent (Evans & Mitchell, 2011; Zhang et al., 2012).

Additional data that constrain the paleogeographic position of Laurentia from the time just following the Trans-Hudson orogeny can test the hypothesis of the unity of Laurentia’s Archean provinces, establish the position of the newly amalgamated Laurentia, and thereby enable tests of hypothesized connections with

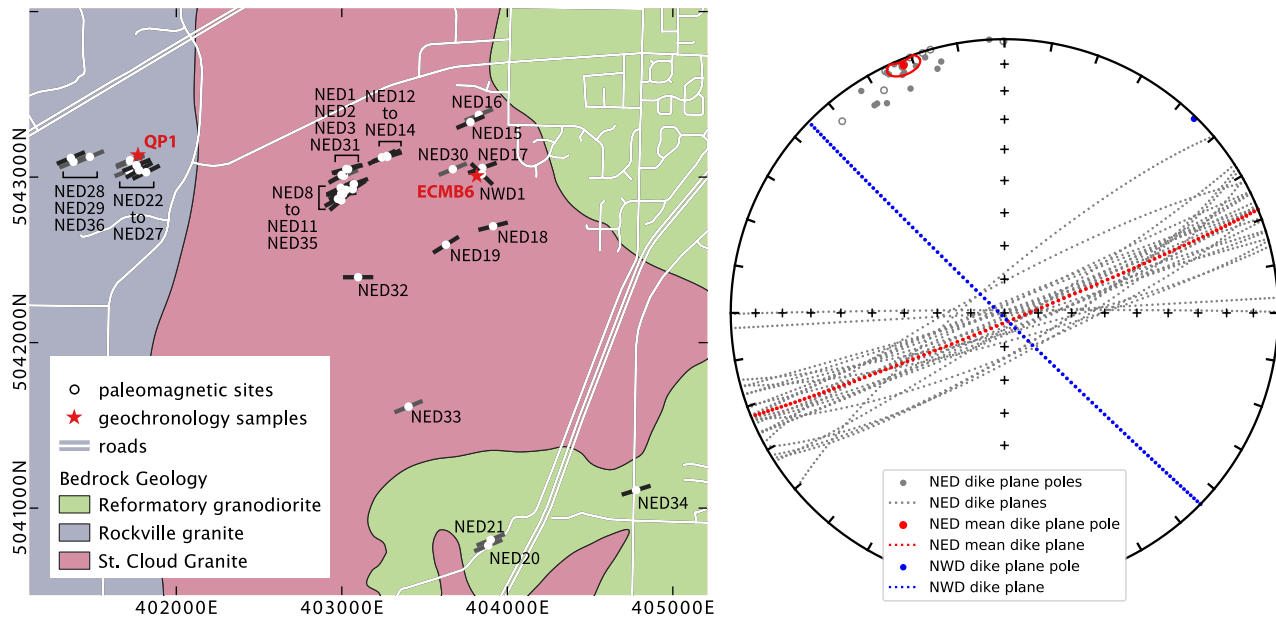


**Figure 2.** Left panel: Locations of paleomagnetic sites of the northeast-trending dikes (NED) and a northwest-trending dike (NWD) within the Rockville Granite, Reformatory Granodiorite and St. Cloud Granite of the East-Central Minnesota Batholith (ECMB) (bedrock geology from Boerboom et al. (1995) and shown in UTM zone 15°N WGS 84 coordinate reference system such that each axis tick is 1 km). Within regions of the mapped St. Cloud Granite there is more complex interfingering of that granite with the Reformatory Granodiorite than is shown. The strikes of the dikes are shown as lines (black when measured on that dike; gray when using the overall mean orientation from the measured NED dikes). The location of the QP1 and ECMB6 geochronology samples are shown. The ECMB4 geochronology sample was collected ~18 km SW of the western edge of the map, in the Richmond Granite which cross-cuts the Rockville Granite and is younger than the NED dikes. Right panel: The orientations of dikes. Each individual dike orientation is the mean of multiple measurements on that dike. The mean of the poles to the NED planes is shown with a red dot and a 95% confidence ellipse on the mean calculated with Fisher statistics. This confidence ellipse intersects the equator indicating that the mean plane cannot be distinguished from vertical.

other cratons. This study develops a new paleomagnetic pole for Laurentia from *ca.* 1,780 Ma diabase dikes of the East-Central Minnesota Batholith (ECMB) that provides such constraints.

## 2. Geologic Setting

Coeval with collisional orogenesis between the assembling Archean provinces that formed Laurentia's core was the *ca.* 1,860 to 1,820 Ma accretionary Penokean orogeny along the southern margin of the Superior Province (Figure 1; Schulz & Cannon, 2007). Penokean orogenesis resulted from island-arc and microcontinent collisions with the Superior Province that led to metamorphism of Superior Province lithologies and development of a foreland basin (Holm et al., 2019; Schulz & Cannon, 2007). Following the Penokean orogeny, there was voluminous magmatism along the southeastern margin of the west Superior Province resulting in the emplacement of the *ca.* 1,780 Ma ECMB and other coeval post-orogenic plutons (Figure 1; Boerboom et al., 2005; Holm et al., 2005; Schmitz et al., 2018). While the ECMB is dominantly comprised of felsic to intermediate plutons, mafic magmas were also generated and commingled with the more abundant felsic magmas throughout the interval of batholith generation as evidenced by mafic enclaves within some of the plutons (Boerboom et al., 2005, 2011; Schmitz et al., 2018). Mafic melt within the ECMB also led to the emplacement of a set of near-vertical northeast-trending diabase dikes (Figure 2; Boerboom et al., 2005). The dikes have chilled margins and are typically 1–3 m wide with widths up to 8 meters (Boerboom et al., 2005). As with the granites they intrude, the dikes have primary igneous texture and no metamorphic fabric (Boerboom et al., 2005). They have experienced variable low-grade alteration such as albitization and sericitization of plagioclase and the formation of pyrrhotite. These diabase dikes are present within all of the granitoid units of the ECMB (e.g., St. Cloud Granite, Rockville Granite, and Reformatory Granodiorite; Figure 2) with the exception of the youngest Richmond Granite. Throughout the field area, the dikes are exposed both in glacially-polished pavement outcrops and in numerous inactive and active dimension stone granite quarries. Northeast-trending diabase dikes are present in all of the quarries in the

Rockville Granite, St. Cloud Granite as well as in the Reformatory granodiorite, regardless of the size of the quarry, as well as in many natural bedrock outcrops. In many of the old inactive quarries, the north and/or south quarry walls are marked by the planar surface of a diabase dike contact, where the rock naturally separates, often resulting in elongated northeast-southwest shapes to the quarry pits. In contrast, no diabase dikes have been found in the quarries or natural exposures of the Richmond granite. Although this granite does not contain as many quarries and there are fewer natural outcrops, the lack of diabase dikes contrasts sharply with the numerous dikes present in the other nearby granites, where an equivalent exposed surface area would contain numerous diabase dikes. This absence indicates that the younger Richmond Granite post-dates the intrusion of the diabase dikes into the St. Cloud Granite, Rockville Granite, and Reformatory Granodiorite.

There are also quartz-feldspar porphyry dikes with the same northeast-trending direction as the diabase dikes found in all the granitoids also with the exception of the Richmond Granite (Boerboom et al., 2005). These porphyritic microgranite dikes have chilled, and locally flow-banded, margins. One has been observed to have intruded into a northeast-trending diabase dike and another has textures consistent with commingling of magmas between the felsic dike and adjacent diabase dike indicative of synchronous emplacement (Boerboom & Holm, 2000). The Richmond Granite has trachytoid magmatic fabric defined by aligned potassium-feldspar phenocrysts that share the same orientation with the northeast-trending dikes (Boerboom & Holm, 2000), indicating that this orientation is associated with a persistent regional stress field throughout the interval of magma emplacement and dike formation. These field relationships indicate that the quartz-feldspar porphyry and diabase dikes are comagmatic with the batholith. The diabase dikes are constrained to be younger than the St. Cloud Granite (new U-Pb date of  $1,781.44 \pm 0.51$  Ma;  $2\sigma$  analytical uncertainty) which they pervasively intrude, older than the Richmond Granite (new U-Pb date of  $1,776.76 \pm 0.49$  Ma) in which they are absent, and similar in age to the quartz-feldspar porphyry dikes (new U-Pb date of  $1,780.78 \pm 0.45$  Ma).

### 3. Paleomagnetic Methods and Results

Oriented samples for paleomagnetism were collected and analyzed from 36 of the northeast-trending dikes of the ECMB and one northwest-trending dike (Figure 2). Each sampled dike constituted a paleomagnetic site in our site naming scheme. These sites were concentrated in and around Stearns County Quarry Park near the city of St. Cloud (Figure 2). Samples were collected from the dikes with a gas-powered drill and oriented in the field with a Pomeroy orienting fixture. The azimuthal orientations of the cores were determined either through sun or magnetic compass depending on cloud cover. Sun compass directions were preferentially used when available. When magnetic compass data were used they were corrected for local magnetic declination using the International Geomagnetic Reference Field model (Thébault et al., 2015). Specimens from the oriented samples were analyzed in the UC Berkeley Paleomagnetism lab using a 2G DC-SQUID magnetometer. Samples either underwent stepwise alternating field (AF) or thermal demagnetization. Thermal demagnetization was accomplished using an ASC thermal demagnetizer (residual fields < 10 nT). AF demagnetization was conducted with inline coils that utilize a Crest Amplifier paired with an Adwin controller to develop a well-controlled waveform. All paleomagnetic data developed in this study are available at the measurement level in the MagIC database (<https://www.earthref.org/MagIC/doi/10.1029/2021TC006751>).

Typical behaviors of sample remanence during demagnetization are illustrated for representative specimens in Figure 3. AF demagnetization data typically reveal three components: a small low-coercivity component approximately aligned with Earth's present local field in the study region that was typically removed below 10 mT; a medium-coercivity component that is steep and was dominantly removed between 10 and 60 mT; and a high-coercivity component that was subsequently removed incompletely as demagnetization progressed to 130 mT. These components are present to varying degrees within individual specimens (Figure 3).

Sister specimens from some samples underwent thermal and AF demagnetization which provides additional insight into the carriers of the components through comparison of the thermal and AF demagnetization spectra (such as NED2-8 in Figure 3). These data reveal that the low-coercivity component direction is

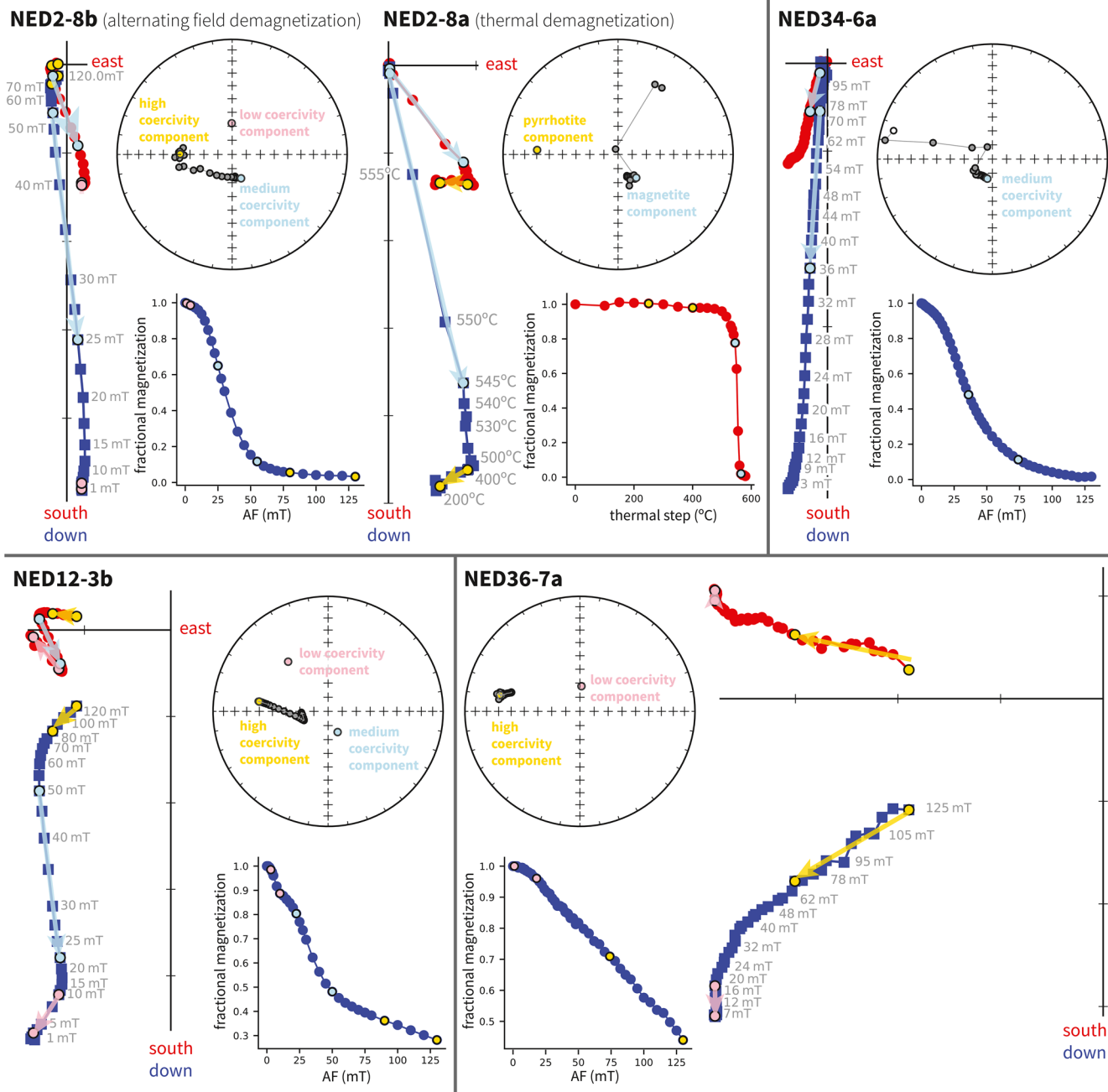


**Figure 3.** Paleomagnetic data from East-Central Minnesota Batholith (ECMB) northeast-trending diabase dikes are shown in geographic coordinates on vector component plots, measurement-level equal area plots and magnetization magnitude plots (developed using PmagPy software; Tauxe et al., 2016). Least squares fits to the data are shown with colored arrows on the vector component plots, colored directions on the equal area plots, and as colored end-points on the magnetization magnitude plots (pink for low-coercivity; blue for medium-coercivity; yellow for high-coercivity). Specimens NED2-8a and NED2-8b are from the same core sample and were analyzed via thermal and alternating field (AF) demagnetization respectively. These data from sample NED2-8 reveal the steep medium-coercivity component to thermally unblock at temperatures characteristic of remanence held by magnetite and the high-coercivity component to thermally unblock at temperatures characteristic of remanence held by pyrrhotite. Specimen NED34-6a is dominated by the steep medium-coercivity component. The medium-coercivity component is well-resolved in specimen NED12-3b which also has a substantial high-coercivity component. The high-coercivity component dominates the remanence of specimen NED36-7a such that no medium-coercivity component can be resolved.

removed at the lowest unblocking temperatures up to 150°C. This behavior, as well as the typical direction, is most consistent with the component being a viscous overprint acquired in Earth's geomagnetic field. The direction of the high-coercivity component is removed through thermal demagnetization between 250°C and 350°C—consistent with its being held by monoclinic pyrrhotite. The direction of this magnetization held by pyrrhotite is aligned with the magnetite-held remanence within a northwest-trending dike in the region (discussed in more detail below)—a direction consistent with the position of Laurentia during the time period of *ca.* 1,096 Ma Midcontinent Rift magmatism (Swanson-Hysell et al., 2020). We interpret this high-coercivity component held by pyrrhotite, whose presence is variable in ECMB dikes, to have formed through hydrothermal activity associated with Midcontinent Rift magmatism such as that represented by the emplacement of the northwest-trending dike. The pyrrhotite thereby carries a chemical remanent magnetization.

In some specimens, the low-coercivity component is much larger and has a direction that is distinct from the present local field. It is likely that these samples acquired an isothermal remanent magnetization associated with quarrying operations or lightning strikes. This behavior can be prevalent throughout a site or can be present in just some samples from a given site. In many cases, these low-coercivity overprints can be removed through AF demagnetization and the medium-coercivity and/or high-coercivity components can be subsequently isolated. In some instances, however, these large and dominantly low-coercivity overprints extend to higher coercivities preventing the isolation of other components.

The medium-coercivity component direction is dominantly removed through thermal demagnetization between 515°C and 565°C consistent with it being held by low-Ti titanomagnetite. This direction was recovered with site mean direction uncertainty less than 8° ( $\alpha_{95} < 8^\circ$ ) for 23 sites (Table 1). We interpret this component to be a primary thermal remanence acquired at the time of dike emplacement as part of the *ca.* 1,780 Ma ECMB. This interpretation gains support from the rock magnetic data, an inverse baked contact test, and thermochronology data that support an emplacement temperature well below the blocking temperature of magnetite and a mild subsequent thermal history—as discussed in more detail below.

### 3.1. Magnetic Mineralogy Constraints From Low-Temperature Magnetometry

To gain additional insight into the magnetic mineralogy of the dikes, a Magnetic Properties Measurement System (MPMS) at the Institute for Rock Magnetism was used to conduct low-temperature remanence experiments. In the field-cooled (FC) experiments shown in Figure 4, the magnetization was measured upon warming following the specimen having cooled in an applied field of 2.5 T from 300 to 10 K. In the zero-field-cooled (ZFC) experiment, a low-temperature saturation isothermal remanence (LTSIRM) of 2.5 T was applied at 10 K after the specimen cooled in a (near-)zero field. In the room-temperature saturation isothermal remanence (RTSIRM) experiment, the sample was pulsed with a 2.5 T field at room temperature (~300 K) and then cooled to 10 K and warmed back to room temperature in a (near-)zero field. These experiments reveal that sister specimens to paleomagnetic specimens whose remanence is dominated by the medium-coercivity component without an appreciable high-coercivity component have strong expressions of the ~120 K Verwey transition as expected for a ferromagnetic mineralogy of well-preserved low-Ti titanomagnetite (NED34-6c in Figure 4; Feinberg et al., 2015; Verwey, 1939). In contrast, specimens from samples that have a larger contribution of the high-coercivity component have weaker saturation magnetization, minor expression of the Verwey transition, and the presence of monoclinic pyrrhotite as evidenced through the ~30 K Besnus transition (NED36-8c in Figure 4; Besnus and Meyer, 1964; Feinberg et al., 2015). Samples with a smaller contribution of the high-coercivity component superimposed on the medium-coercivity component have intermediate behavior with a minor expression of the Besnus transition and a more prominent Verwey transition (NED2-8c in Figure 4). These results support the interpretation that the medium-coercivity component is held by primary unaltered (titano)magnetite and that the high-coercivity component is the result of subsequent alteration that resulted in degradation of magnetite and formation of pyrrhotite.

### 3.2. Baked Contact Test

One northwest-trending dike is exposed and was sampled within the study region as site NWD1 (Figure 2). The magnetization direction of this dike indicates that it is associated with the main stage of the

**Table 1**  
*Summary of Site Level Paleomagnetic Data*

Site	Site lat	Site lon	<i>n</i>	Dec	Inc	k	R	$\alpha_{95}$	VGP lat	VGP lon
<i>northeast-trending dike magnetite-component site means</i>										
NED1	45.53423	265.75804	8	157.6	74.7	380	7.98	2.8	18.4	276.9
NED2	45.53421	265.75816	8	172.3	74.9	420	7.98	2.7	17.4	269.6
NED5	45.53309	265.75803	6	170.3	79.0	213	5.98	4.6	24.5	269.6
NED6	45.53299	265.75773	9	197.8	73.6	183	8.96	3.8	16.1	256.5
NED7	45.53288	265.75767	5	266.3	81.3	204	4.98	5.4	42.0	242.6
NED8	45.53286	265.75782	7	202.6	78.6	423	6.99	2.9	24.8	256.6
NED9	45.53314	265.75855	7	191.1	71.5	90	6.93	6.4	12.2	259.5
NED10	45.53259	265.75742	6	199.7	73.3	324	5.98	3.7	15.8	255.4
NED11	45.53252	265.75768	7	166.1	75.1	391	6.98	3.1	18.1	272.6
NED12	45.53489	265.76076	6	179.5	73.0	374	5.99	3.5	14.1	266.0
NED13	45.53497	265.76113	7	169.1	73.9	199	6.97	4.3	15.9	271.4
NED14	45.53492	265.76119	6	193.0	70.0	217	5.98	4.6	10.1	258.0
NED15	45.53688	265.76758	8	175.8	77.7	604	7.99	2.3	22.0	267.6
NED16	45.53728	265.76822	5	185.1	78.6	449	4.99	3.6	23.6	263.7
NED18	45.53124	265.76945	6	134.7	81.7	159	5.97	5.3	33.2	279.5
NED23	45.53398	265.74200	7	193.0	76.4	411	6.99	3.0	20.2	259.7
NED25	45.53396	265.74119	4	135.4	80.7	334	3.99	5.0	31.5	280.6
NED26	45.53445	265.74129	5	151.1	73.4	572	4.99	3.2	17.4	280.8
NED28	45.53467	265.73817	4	157.8	73.8	145	3.98	7.7	16.9	277.2
NED29	45.53438	265.73690	8	219.0	76.7	119	7.94	5.1	24.4	248.6
NED31	45.53385	265.75785	3	184.7	69.4	1,730	3.00	3.0	8.7	262.9
NED34	45.51700	265.78083	8	185.9	77.0	362	7.98	2.9	20.8	263.1
NED35	45.53320	265.75761	8	166.4	74.7	261	7.97	3.4	17.4	272.6
<b>mean pole: pole longitude: 265.8; pole latitude: 20.4; <math>A_{95}</math>: 4.5; K: 45.6 N: 23</b>										
<i>northwest-trending dike magnetite-component site mean</i>										
NWD1	45.53407	265.76852	9	293.4	41.6	66	8.88	6.4	32.9	177.5

*Notes:* site lat–latitude of site (°; WGS84); site lon–longitude of site (°; WGS84) *n*–number of samples analyzed and included in the site mean; dec–tilt-correction mean declination for the site; inc–tilt-correction mean inclination for the site; k–Fisher precision parameter; R–resultant vector length;  $\alpha_{95}$ –95% confidence limit in degrees; VGP lat–latitude of the virtual geomagnetic pole for the site; VGP lon–longitude of the virtual geomagnetic pole for the site.

Midcontinent Rift (*ca.* 1,096 Ma) as it has a normal polarity and an inclination consistent with that time interval of Midcontinent Rift volcanism (Figure 5; Swanson-Hysell et al., 2020). The dike cross-cuts one of the northeast-trending dikes (NED17) allowing for a baked contact test (Figures 2 and 5). The baked contact test is positive with a distinct direction in the northeast-trending dike (corresponding to the remanence direction seen throughout the northeast-trending dikes of the ECMB) with its magnetite remanence becoming progressively overprinted by the northwest-trending dike up to the contact (Figure 5). This positive baked contact test indicates that the northeast-trending ECMB dikes have not been overprinted since the northwest-trending dike was emplaced (*ca.* 1,096 Ma). This positive baked contact test for the northwest-trending dike constitutes what is referred to as a positive “inverse” baked contact test for the northeast-trending dike remanence—it constrains the remanence to be more ancient than the *ca.* 1.1 Ga Mesoproterozoic northwest-trending dike, but does not provide a constraint back to the Paleoproterozoic time of dike emplacement. Given that the host rocks for the northeast-trending dikes are of a very similar age to the dikes themselves there is not the possibility of a Paleoproterozoic baked contact test. In contrast to the dikes, stable and consistent remanence directions were not recovered from pilot sites in ECMB granites.

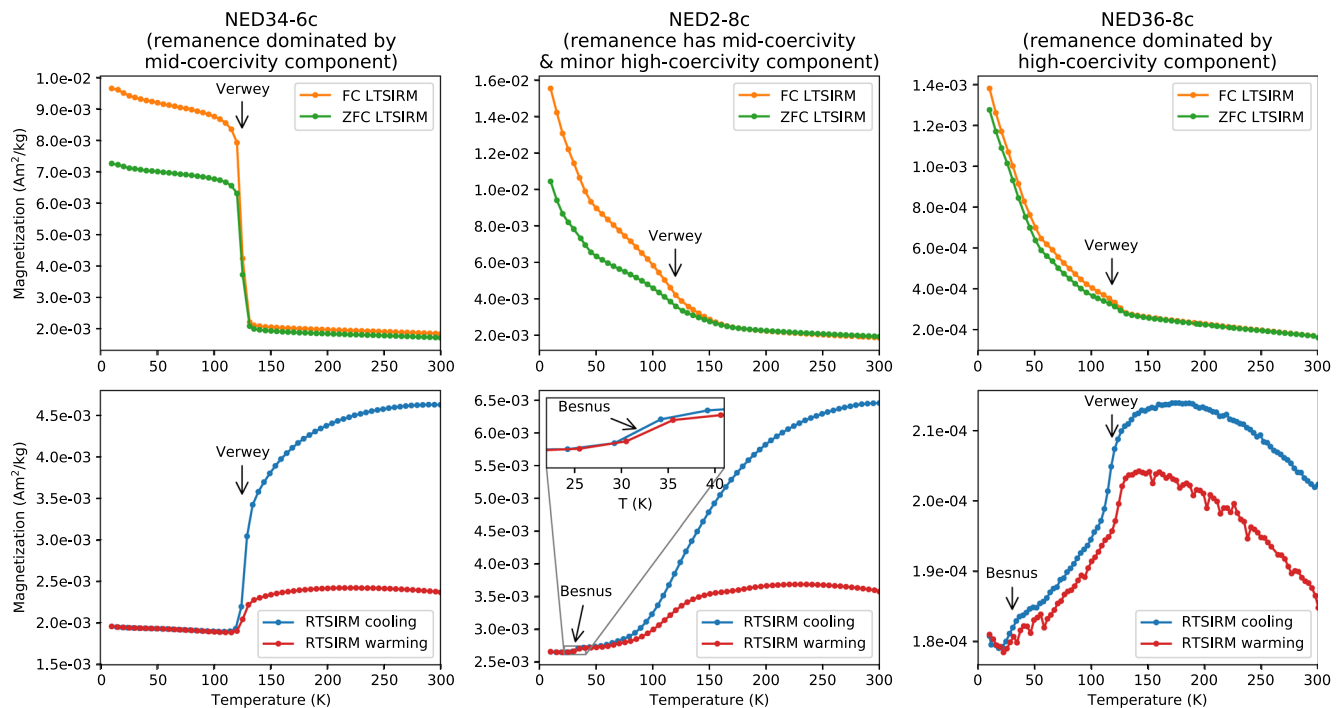


**Figure 4.** Low-temperature remanence experiment data. The specimen from a sample whose natural remanent magnetization is dominated by the medium-coercivity component (NED34-6c) has behavior dominated by magnetite as evidenced through the response across the ~120 K Verwey transition. The specimen from a sample whose natural remanence is dominated by the high-coercivity component (NED36-8c) has weaker magnetization, a relatively minor expression of the Verwey transition, and expression of the ~32 K Besnus transition that indicates the presence of monoclinic pyrrhotite. The specimen whose natural remanence has a well-resolved medium-coercivity component with a minor high-coercivity component (NED2-8c) has intermediate behavior with a Verwey transition that is not as suppressed as in NED36-8c with a minor, but resolvable, Besnus transition (see inset). FC: field-cooled; ZFC: zero-field-cooled; LTSIRM: low-temperature saturation isothermal remanence magnetization; RTSIRM: room-temperature saturation isothermal remanence magnetization.

The high-coercivity remanence direction held by pyrrhotite in some of the northeast-trending dikes is aligned with the remanence direction of the northwest-trending dike. While the thermal effect of the northwest-trending dike was limited to a few meters on either side of it as evidenced through the baked contact test (Figure 5), there was more widespread hydrothermal alteration associated with Midcontinent Rift magmatic activity that led to the formation of pyrrhotite and an associated chemical remanent magnetization. In the majority of the northeast-trending dikes, the original magnetite is well-preserved (e.g., NED34 of Figures 3 and 4) while other dikes experienced variable magnetite alteration and the formation of secondary pyrrhotite (e.g., NED36 of Figures 3 and 4). These components can be separated through progressive demagnetization (e.g., NED12 of Figure 3) enabling the thermal remanent magnetization held by magnetite to be used to determine site mean directions and calculate a paleomagnetic pole (Figure 6).

### 3.3. Paleomagnetic Pole

The site mean directions determined from the magnetite remanence component can be converted to virtual geomagnetic poles and then used to calculate a mean paleomagnetic pole for the ECMB diabase dikes (pole longitude: 265.8°; pole latitude: 20.4°;  $A_{95}$ : 4.5°; K: 45.6 N: 23; Figure 6). These 23 virtual geomagnetic poles have a distribution consistent with a Fisher distribution as determined through the Fisher et al. (1987) goodness-of-fit method. The  $A_{95}$  uncertainty on the mean pole position of 4.5° is within the bounds of reliability proposed by Deenen et al. (2011). It is well below the  $A_{95}$ -max value proposed to establish a well-determined mean for 23 sites (11.4°) and above the  $A_{95}$ -min value (3.4°) consistent with the site directions having sufficiently sampled secular variation of the geomagnetic field.

In a massive host rock such as the ECMB plutons without preferential bedding or foliation, it is expected that lithospheric stresses will lead to the emplacement of near vertical dikes. Dike plane orientations were measured on each dike for which there was sufficient three-dimensional exposure. Multiple measurements



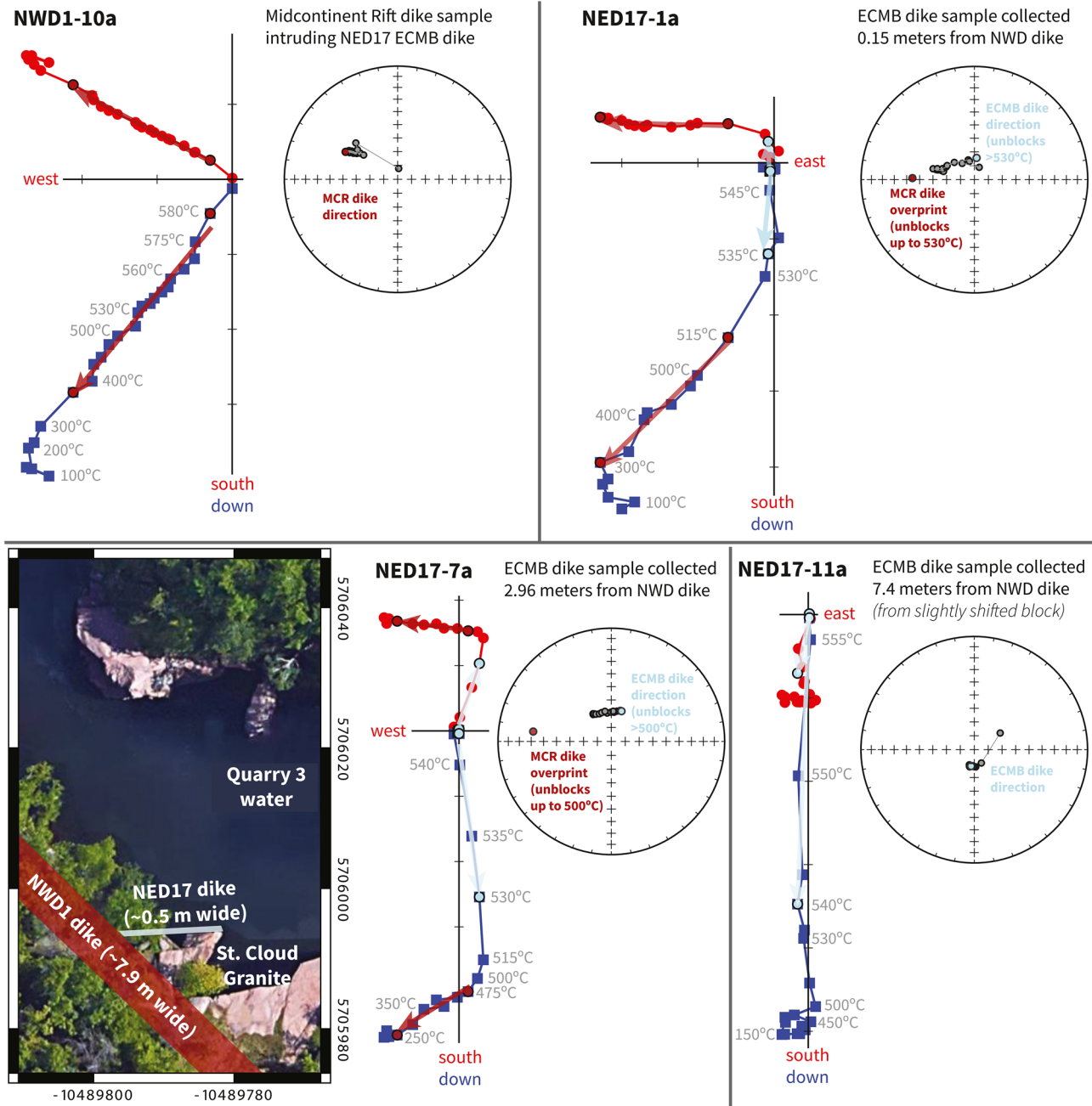


**Figure 5.** Results from a positive baked contact test where a northwest-trending dike (site NWD1) cross-cuts a northeast-trending dike (site NED17). The NWD1 dike has a direction indicating that it formed during the *ca.* 1,096 Ma main stage of rift volcanism. Close to the NWD1 dike the NED17 is nearly fully overprinted (NED17-1a). Further from NWD1 there are partial thermal overprints (NED17-7a) that by ~7 meters from the cross-cutting dike are not resolvable (NED17-11a). Note that blocks from this dike were slightly shifted due to quarrying operations which does not bear on the significance of the positive test, but has led to the exclusion of the result from the site mean compilation and overall pole.

were made for each dike to constrain their orientation. The mean strike calculated from 17 dike orientations is  $067^\circ$  and the mean dip is  $88^\circ$  (Figure 2). The  $\alpha_{95}$  uncertainty associated with the Fisher mean for the poles to these dike orientation planes (i.e., the lines perpendicular to the planes) is  $4.7^\circ$  which means that the overall orientation of the planes is statistically indistinguishable from vertical (Figure 2). Due to this verticality, we interpret the exhumation of the ECMB plutons to have not resulted in appreciable tilting since dike emplacement and do not apply a tilt correction to the paleomagnetic data.

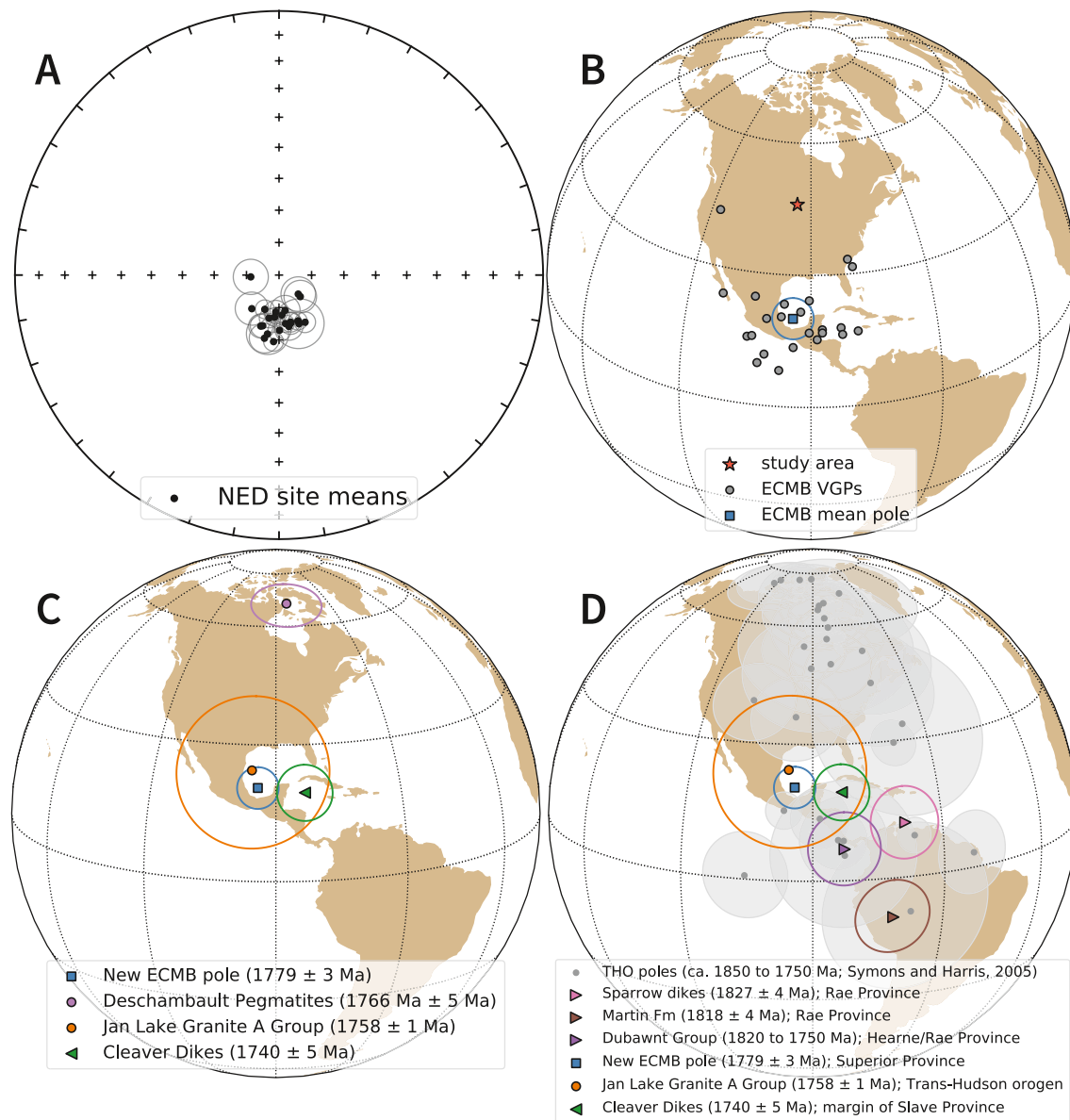


**Figure 6.** (a) Site mean directions for the magnetite remanence of the northeast-trending (NED) East-Central Minnesota Batholith (ECMB) diabase dikes with  $\alpha_{95} < 8^\circ$ . (b) Virtual geomagnetic poles (VGPs) calculated from these site means and the overall mean paleomagnetic pole for the ECMB dikes. (c) Comparison between the new ECMB paleomagnetic pole and other ca. 1,780–1,740 Ma poles for Laurentia. (d) Comparison of poles from Laurentia's provinces from 1,830 to 1740 Ma from Evans et al. (2021) as well as poles from the Trans-Hudson orogen (THO; gray; Symons & Harris, 2005) with the new ECMB pole.

#### 4. Geochronology Methods and Results

The field relationships show the diabase dikes to be younger than the Rockville Granite, Reformatory Granodiorite and the St. Cloud Granite which they pervasively intrude and to be older than the Richmond Granite where they are absent (Boerboom et al., 2005). Holm et al. (2005) developed U-Pb dates calculated as concordia intercept dates from these intrusions. The dates reported by Holm et al. (2005) for granites intruded by the dikes are  $1,783 \pm 11$  Ma for the Reformatory Granodiorite,  $1,780 \pm 7$  Ma for the Rockville Granite and  $1,779 \pm 5$  Ma for the St. Cloud Granite. The younger cross-cutting Richmond Granite has a date of  $1,772 \pm 3$  Ma (Holm et al., 2005). An age of  $1,774 \pm 7$  Ma for one of the quartz-feldspar porphyry dikes developed by Holm et al. (2005) is consistent with this interpretation of these dikes being older than the Richmond Granite (and younger than the granites they intrude). While the dates published in Holm et al. (2005)

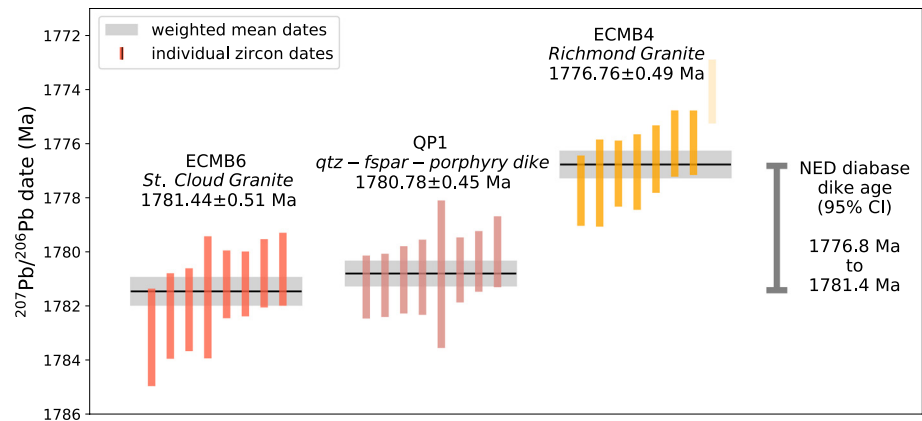


**Figure 7.** U-Pb dates for East-Central Minnesota Batholith (ECMB) samples. Weighted mean dates (horizontal lines) are calculated from individual zircon dates (vertical bars). The northeast-trending (NED) diabase dikes intrude the St. Cloud Granite such that the ECMB6 weighted mean date of  $1,781.44 \pm 0.51$  Ma is a maximum age. The quartz-feldspar porphyry dikes (one of which was sampled as QP1) also intrude the St. Cloud Granite and are parallel to the NED diabase dikes. Neither the quartz-porphry dikes nor the diabase dikes intrude the younger cross-cutting Richmond Granite such that the ECMB4 weighted mean date of  $1,776.76 \pm 0.49$  Ma provides a minimum age for the dikes. Details for the weighted mean dates are given in Table 2 and individual zircon data are in the Supporting Information.

are valuable constraints and are consistent with the field relationships, they are of lower precision than what is possible with modern analytical approaches and therefore lead to overlapping uncertainties. Higher precision constraints resulting from methods that apply ion-exchange separation with low blank analyses of chemically abraded single zircon grains can test the field relationship interpretations and provide more confidence in the overall age constraints.

To further constrain the age of the northeast-trending diabase dikes, we developed new isotope dilution-thermal ionization mass spectrometry (ID-TIMS) U-Pb zircon dates from the St. Cloud Granite that host the dikes (sample ECMB6), the Richmond Granite from which the dikes are absent (sample ECMB4), and from a northeast-trending quartz-feldspar porphyry dike (sample QP1) that is likely coeval with the diabase dikes (Figures 2 and 7). Zircon crystals were chemically abraded prior to analysis of single zircon grains by ID-TIMS at the Boise State Isotope Geology Laboratory (detailed geochronology methods are provided in the supporting information). Weighted mean dates were calculated from multiple single zircon dates (Figure 7; Table 2). While chemical abrasion served to reduce Pb-loss and resulted in concordant analyses, some grains have persistent Pb-loss and are discordant (Figure S1). As a result, we calculate weighted mean  $^{207}\text{Pb}/^{206}\text{Pb}$  dates rather than  $^{206}\text{Pb}/^{238}\text{U}$  dates (Figure 7; Table 2). These  $^{207}\text{Pb}/^{206}\text{Pb}$  dates are  $1,781.44 \pm 0.51$  Ma ( $2\sigma$  analytical uncertainty; MSWD = 1.24;  $n = 8$ ) for the St. Cloud Granite (ECMB6) and  $1,776.76 \pm 0.49$  Ma (MSWD = 1.15;  $n = 7$ ) for the Richmond Granite (ECMB4; Figure 7). The date for the sampled quartz-feldspar porphyry dike (QP1) of  $1,780.78 \pm 0.45$  Ma (MSWD = 0.53;  $n = 8$ ) is between these two dates as expected on the basis of field relationships. Taking into account the analytical uncertainty on the maximum and minimum age constraints, the diabase dikes are younger than the  $1,781.44 \pm 0.51$  Ma

**Table 2**  
Summary of ID-TIMS  $^{207}\text{Pb}/^{206}\text{Pb}$  East-Central Minnesota Batholith Zircon Dates

Sample	Unit	Latitude		$^{207}\text{Pb}/^{206}\text{Pb}$		Uncertainty ( $2\sigma$ )		
		Longitude (WGS84)		Date (Ma)	X	Z	MSWD	n/N
ECMB6	St. Cloud granite	45.53396°N 94.23187° W		1,781.44	0.51	2.4	1.24	8/8
QP1	Quartz-feldspar porphyry dike	45.53481°N 94.25811° W		1,780.78	0.45	2.4	0.53	8/8
ECMB4	Richmond granite	45.44343°N 94.48360° W		1,776.76	0.49	2.4	1.15	7/8

Notes: X is  $2\sigma$  analytical uncertainty; Z is  $2\sigma$  uncertainty including decay constant uncertainty. This Z uncertainty needs to be utilized when comparing to dates using other decay systems (e.g.,  $^{40}\text{Ar}/^{39}\text{Ar}$ ,  $^{187}\text{Re}/^{187}\text{Os}$ ); MSWD is the mean squared weighted deviation; n is the number of individual zircon dates included in the calculated sample mean date; N is the number of individual zircons analyzed for the sample.

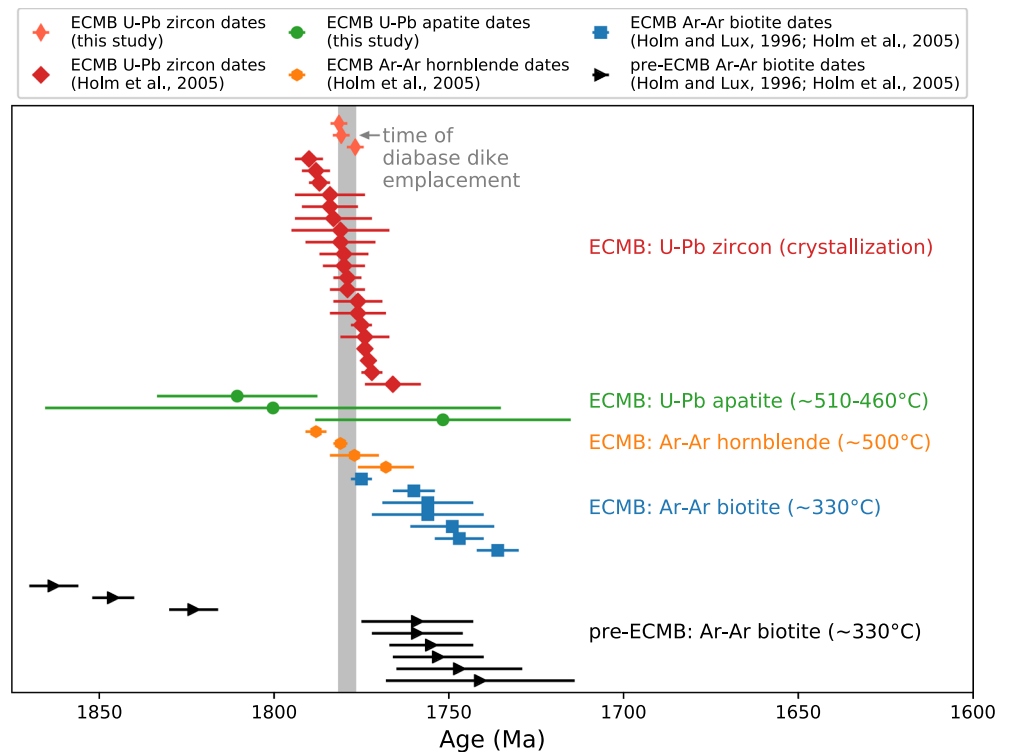


**Figure 8.** Summary of U-Pb zircon dates, U-Pb apatite dates, Ar-Ar hornblende, and Ar-Ar biotite dates from the East-Central Minnesota batholith (ECMB) from this study, Holm and Lux (1996) and Holm et al. (2005). Approximate closure temperatures associated with the thermochronometers are labeled next to the relevant data. That the U-Pb apatite and Ar-Ar hornblende dates are indistinguishable from the U-Pb zircon crystallization dates indicates that the plutons were emplaced at upper middle to upper crustal levels. The Ar-Ar biotite dates from both the ECMB plutons and older host rock lithologies indicate exhumation within ~20 million years to shallower depths and a lack of regional tectonothermal activity over the following 1.75 billion years.

St. Cloud Granite and older than the  $1,776.76 \pm 0.49$  Ma Richmond Granite. If one assumes a uniform probability of diabase emplacement timing between the maximum and minimum age constraints that have normally distributed uncertainties, the 95% confidence interval can be estimated through Monte Carlo simulation. Applying this approach gives a mean age of 1,779.1 Ma with 95% confidence interval (CI) bounds of 1,776.8–1,781.4 Ma. We can succinctly state the age of the northeast-trending ECMB diabase dikes as being  $1,779.1 \pm 2.3$  Ma (95% CI).

## 5. Thermochronology Methods and Results

While the U-Pb zircon dates constrain the crystallization ages of the ECMB intrusions, additional insight into the thermal history of the batholith can help with interpretation of the paleomagnetic data given that the thermal remanent magnetization of magnetite will be blocked at temperatures below 580°C. As discussed below, existing Ar-Ar dates on hornblende and biotite from the ECMB provide valuable constraints in this regard (Figure 8). In this study, we also develop new U-Pb apatite dates from three ECMB granites (ECMB1, the Isle Granite; ECMB3, the Rockville Granite; ECMB4, the Richmond Granite). In contrast to zircon, for which the temperatures of appreciable Pb diffusion exceed the liquidus of granite (Cherniak & Watson, 2001), the temperature window for closure of the U-Pb system in apatite is much lower (~510°C–460°C; Smye et al., 2018). As a result, U-Pb dates of apatite serve as a thermochronometer at moderately high temperatures (Chamberlain & Bowring, 2001; Cochrane et al., 2014; Schoene & Bowring, 2007). These temperatures are of particular relevance to the interpretation of the paleomagnetic data as they are lower than, or correspond with, the blocking temperature of low-Ti titanomagnetite. If a pluton was emplaced at depths where temperatures exceed the closure temperature of apatite, or if it experienced

prolonged reheating, the U-Pb apatite dates would be appreciably younger than the U-Pb zircon crystallization dates.

U-Pb data were developed from apatite grains separated from ECMB granites through laser ablation inductively coupled plasma mass spectrometry (LA-ICP-MS) at UC Santa Barbara (method details are provided in the supporting information). In contrast to zircon, apatite incorporates significant Pb at the time of crystallization. As a result of this elevated common Pb, U-Pb dates were determined through the calculation of Tera-Wasserburg concordia lower intercept dates where the upper intercept corresponds to the ratio of initial  $^{207}\text{Pb}/^{206}\text{Pb}$  and the lower intercept is the  $^{206}\text{Pb}/^{238}\text{U}$  date (following the method of Ludwig, 1998 as implemented in the IsoplotR software of Vermeesch, 2018; Figure S2). Sample ECMB1 is from the Isle Granite which has a U-Pb zircon date of  $1,779 \pm 26$  Ma (Holm et al., 2005). The U-Pb apatite date for ECMB1 is  $1,800.3 \pm 33.4/65.2$  Ma where the first uncertainty is the  $2\sigma$  analytical uncertainty and the second uncertainty is 95% confidence interval for the date that incorporates overdispersion (this uncertainty scheme will be used for all the presented apatite dates). This U-Pb apatite date is therefore indistinguishable from the U-Pb crystallization date (Figure 8). Sample ECMB3 is from the Rockville Granite which has a U-Pb zircon date of  $1,780 \pm 7$  Ma (Holm et al., 2005). The U-Pb apatite date for ECMB3 is  $1,810.5 \pm 16.2/23.0$  Ma. The youngest end of the overdispersion uncertainty range is very similar to (albeit just slightly older than) the U-Pb zircon date. It is not geologically reasonable for the U-Pb apatite date to be older than the U-Pb zircon date. This result therefore suggests that the U-Pb apatite date uncertainty is a slight underestimate with the U-Pb apatite system having closed just after the time of zircon crystallization as constrained through the U-Pb zircon date. Sample ECMB4 is from the Richmond Granite for which we have developed a new ID-TIMS U-Pb zircon date of  $1,776.76 \pm 0.49$  Ma. The U-Pb apatite date for ECMB4 is  $1,751.7 \pm 17.8/36.6$  Ma which is indistinguishable from the U-Pb zircon date (Figure 8).

Pb closure temperatures ( $T_c$ ) for the analyzed apatite grains can be estimated with the Dodson (1973) approach assuming a cylindrical geometry with half-widths as the characteristic diffusion length. Apatite grain sizes are similar across the three dated specimens; they typically are 100–200  $\mu\text{m}$  long and 50–75  $\mu\text{m}$  wide. Using the Pb diffusivity values of Cherniak et al. (1991), a cooling rate of 20°C/Myr results in closure temperatures of 463°C–473°C for these grain sizes. A more rapid cooling rate is likely for the batholith given the similarity of the U-Pb apatite dates with the U-Pb zircon dates. A cooling rate of 100°C/Myr from crystallization to apatite closure temperatures results in closure temperatures of 493°C–505°C.

Overall, these data indicate that the samples cooled through the  $\sim 500^\circ\text{C}$  closure temperatures of the U-Pb apatite system near the time of zircon crystallization consistent with rapid cooling rates of the plutons (Figure 8). Additionally, there has not been significant diffusion due to later tectonothermal events. As discussed below, this result is consistent with Ar-Ar hornblende dates from the ECMB granites and supports the magnetite remanence being a primary thermal remanent magnetization.

## 6. Discussion

### 6.1. Thermal History of the ECMB and a Primary Interpretation of the ECMB Dike Pole

Prior to the emplacement of the ECMB, Paleoproterozoic host rocks were metamorphosed to amphibolite facies during the Penokean orogeny (Holm & Selverstone, 1990). Emplacement of the ECMB has been hypothesized to be post-orogenic and associated with an interval of extensional collapse of the orogen (Boerboom & Holm, 2000; Holm & Lux, 1996). The Al-in-hornblende igneous barometer was applied to the St. Cloud and Isle Granites of the ECMB by Holm, Darrah, and Lux (1998). This barometer has varying published calibrations. Applying the pressure calibration of Mutch et al. (2016) to the data in Holm, Darrah, and Lux (1998) and assuming a 2.7 g/cm<sup>3</sup> overburden gives an estimated emplacement depth of  $10.8 \pm 1.7$  km for the Freedhem Granodiorite,  $\sim 10.4 \pm 1.7$  km for the Isle Granite and  $13.4 \pm 2.1$  km for the St. Cloud Granite. The calibration of Ague (1997) leads to slightly higher calculated pressures implying depths that are  $\sim 2.3$  km deeper.

Thermochronology data give additional insight into emplacement temperatures (and thereby depth). Both the Ar-Ar hornblende dates published by Holm et al. (2005) and the U-Pb apatite dates developed in this study from ECMB lithologies are indistinguishable from the crystallization ages of the intrusions (Figure 8). The closure temperature for Ar in hornblende is  $\sim 580^\circ\text{C}$ – $490^\circ\text{C}$  (Harrison, 1982). The closure of the U-Pb

system in the dated apatite grains is  $\sim 500^{\circ}\text{C}$ – $460^{\circ}\text{C}$ . The consistency between the U-Pb zircon crystallization and the U-Pb apatite and Ar-Ar hornblende cooling dates indicates that the present-day erosion level of the ECMB was at a shallow enough depth that the crustal temperatures were lower than these closure temperatures at the time of emplacement of the plutons. Geothermal gradients in continental arc settings are typically between  $25^{\circ}\text{C}/\text{km}$  and  $45^{\circ}\text{C}/\text{km}$ —potentially higher at 1.8 Ga (Rothstein & Manning, 2003). Taking a geothermal gradient of  $30^{\circ}\text{C}/\text{km}$  and the closure temperature constraints indicates that the plutons were emplaced at 15 km or shallower in the continental lithosphere. This emplacement depth is consistent with the Al-in-hornblende paleobarometry estimates.

Ar-Ar biotite dates provide insight into even lower temperatures as the system blocks at  $\sim 330^{\circ}\text{C}$  (Grove & Harrison, 1996), well below the blocking temperature of magnetite magnetization in the dikes. Ar-Ar biotite dates from ECMB plutons range from overlapping the crystallization dates to being younger by  $\sim 20$  million years (Figure 8). Ar-Ar biotite dates from older host lithologies to the ECMB are either older than the age of the batholith itself or the same age as the Ar-Ar biotite dates from the batholith (Figure 8). These data suggest that the batholith was emplaced near the upper depth range estimates from the Al-in-hornblende barometry ( $\sim 10$  km) and underwent exhumation to below the  $\sim 330^{\circ}\text{C}$  closure temperature of the K-Ar biotite system soon after emplacement of the plutons. These data also indicate that there has not been reheating or pervasive fluid flow that would have perturbed the Ar-Ar thermochronometers in the granites in the time since initial cooling. The magnetization used to develop the paleomagnetic pole comes from remanence held by low-Ti magnetite that dominantly unblocks between  $540^{\circ}\text{C}$  and  $560^{\circ}\text{C}$  (Figures 3 and 5). The thermochronology results constrain the rocks to have cooled through the magnetite blocking temperatures at the time that the dikes were emplaced within the batholith and to not have experienced reheating that would have perturbed the thermochronometers. These data support an interpretation that the magnetite remanence within the ECMB dikes is a primary thermal remanent magnetization.

These thermochronology data also demonstrate that following the emplacement of the ECMB there were not regional tectonothermal events with the potential to have thermally modified the magnetization of the magnetite within the ECMB diabase dikes. Subsequent Paleoproterozoic Yavapai and Mazatzal accretion occurred to the southeast of the Spirit Lake Tectonic zone on the other side of the Minnesota River Valley promontory ( $\sim 160$  km south of the study region; Figure 1; Holm et al., 2007). In contrast to the north-east-trending dikes in the ECMB, northeast-trending dikes in Wisconsin within *ca.* 1,840 Ma plutons were metamorphosed to amphibolite facies associated with such accretionary orogenesis (Holm et al., 2019). Mazatzal orogeny deformation and metamorphism occurred *ca.* 1,650 to 1,630 Ma within the juvenile accreted island arc of the Wisconsin Magmatic Terrane (Holm, Schneider, & Coath, 1998). The region of the ECMB was not affected by these tectonothermal events (Figure 1, Holm et al., 2005). Holm et al. (2005) proposed that the voluminous ECMB batholith stabilized the continental lithosphere and prevented the region from being modified during subsequent collisions along the margin. This lack of deformation in the region of the ECMB is further supported by the nearly horizontal bedding of *ca.* 1.63 Ga siliciclastic sedimentary rocks on either side of the batholith (Holm, Schneider, & Coath, 1998; Medaris et al., 2021). In southwestern Minnesota, plutons coeval with the ECMB are overlain by the subhorizontal Sioux Quartzite (Figure 1) with the correlative Barron Quartzite of northwestern Wisconsin also being undeformed (Southwick et al., 1986). This lack of deformation contrasts with correlative Baraboo quartzite south of the Spirit Lake Tectonic Zone ( $\sim 400$  km from the ECMB) that underwent compressional deformation during subsequent orogenesis (Holm, Schneider, & Coath, 1998; Medaris et al., 2021). The Yavapai and Mazatzal terranes were intruded by *ca.* 1,470–1,430 Ma granites of the Eastern Granite Rhyolite Province and there is a sizable pluton of this age within accreted Penokean rocks in northern Wisconsin (the *ca.* 1,470 Ma Wolf River batholith; Dewane and Van Schmus, 2007). However, the thermal effects of the Wolf River batholith ( $\sim 370$  km east of the ECMB study area) were limited to a 10–15 km wide contact zone surrounding the intrusion (Holm et al., 2019).

The one major subsequent tectonothermal event in the region for which there is localized evidence in the ECMB is the development of the Midcontinent Rift that initiated *ca.* 1,109 Ma and in which magmatic activity continued to *ca.* 1,084 Ma (Figure 1; Fairchild et al., 2017; Swanson-Hysell et al., 2019). While the main rift axis can be inferred from gravity and aeromagnetic anomaly data to be located  $\sim 75$  km southeast of the study region (Figure 1), the studied northwest-trending dike has a magnetization direction that implies that it was emplaced during Midcontinent Rift development *ca.* 1,096 Ma (Figure 5). The baked contact

test between that dike (NWD1) and the northeast-trending dike that it cross-cuts (NED17), indicates that the thermal effect of the dike emplacement and the Midcontinent Rift in general was localized within the immediate vicinity of that dike (a few meters; Figure 5). However, this Midcontinent Rift magmatic activity did result in local hydrothermal alteration as evidenced by magnetization held by monoclinic pyrrhotite that is variably present through the ECMB dikes and is in the same direction as the magnetization of the northwest-trending dike (Figure 3). This chemical remanent magnetization held by monoclinic pyrrhotite likely formed at relatively low temperatures. Phase relationships in the Fe-S system developed through hydrothermal recrystallization experiments show monoclinic pyrrhotite to form at temperatures below 250°C and likely above 75°C (Kissin & Scott, 1982). While in some sites, this pyrrhotite-forming alteration obscured the primary thermal remanence held by magnetite (e.g., NED36 in Figure 3), in the majority of sites the magnetite remanence direction can be well-resolved (e.g., NED2, NED12 and NED34 in Figure 3). As a result, the paleomagnetic directions used to calculate the paleomagnetic pole shown in Figure 6 are held by (titano)magnetite that recorded a thermal remanent magnetization upon cooling of the diabase dikes. This evidence for variable late Mesoproterozoic hydrothermal alteration of the dikes provides an explanation for Ar-Ar data developed from two northeast-trending diabase dikes that were reported in Boerboom and Holm (2000). These Ar-Ar data did not yield a plateau age, but give whole rock total gas dates that are late Mesoproterozoic in age. An interpretation that these whole rock total gas ages correspond with the age of emplacement is difficult to reconcile with the cogenetic relationship between the diabase dikes, the quartz-feldspar porphyry dikes and the ECMB granites. K-Ar whole-rock ages of 1,570–1,280 Ma from the dikes reported in Hanson (1968) and discussed in Horan et al. (1987) are attributed to partial resetting. The evidence for fluid flow that led to the formation of pyrrhotite *ca.* 1,096 Ma supports the hypothesis put forward by Horan et al. (1987), as well as by Boerboom and Holm (2000), that there was Mesoproterozoic disruption of the K-Ar isotopic system in the dikes such that the Mesoproterozoic Ar-Ar dates are the result of alteration of dikes which are Paleoproterozoic in age. The field relationships indicating that the northeast-trending diabase dikes are comagmatic with ECMB granites is also consistent with whole rock Pb isotope data that reveal very similar arrays implying a *ca.* 1.8 Ga isochron age for both lithologies (Horan et al., 1987).

Overall, the constraints requiring that the ECMB granites were emplaced at depths where the ambient temperature was below the closure of U-Pb apatite and Ar-Ar hornblende systems indicate that the comagmatic diabase dikes would have acquired their magnetization at the time of emplacement. The lack of significant thermal events that could have reset the magnetite magnetization is indicated by the geologic setting, the thermochronology data (including the Paleoproterozoic Ar-Ar biotite dates), and the positive inverse baked contact test. We therefore interpret the pole calculated from the magnetite remanence of the ECMB diabase dikes as a high-quality constraint on the paleogeographic position of Laurentia at the time the dikes intruded ( $1,779.1 \pm 2.3$  Ma). The ECMB diabase dikes pole meets six of the seven criteria for the quality criteria Van der Voo (1990) and the Meert et al. (2020) reliability criteria with the only one not satisfied being due to the lack of dual polarity directions. This single polarity normal polarity is consistent with the polarity of the Cleaver Dykes and the proposal of Irving (2004) that there was a normal geomagnetic superchron that followed the Trans-Hudson orogeny.

## 6.2. Laurentia's Paleomagnetic Poles Following the Trans-Hudson Orogeny

The Trans-Hudson orogeny is a major event in the formation of Laurentia resulting from collision between the Superior province and the Churchill plate consisting of the composite Slave + Rae + Hearne provinces (Corrigan et al., 2009; Hoffman, 1988; Weller & St-Onge, 2017). Geologic data on the timing of Trans-Hudson orogenesis include a  $^{206}\text{Pb}/^{238}\text{U}$  date of  $1,854.2 \pm 1.6$  Ma from the base of a foredeep sedimentary succession on the northern margin of the East Superior province that constrains flexural subsidence associated with Trans-Hudson orogenesis to have initiated at that time (Hodgskiss et al., 2019). This timing of orogenesis is consistent with  $^{207}\text{Pb}/^{206}\text{Pb}$  dates of monazite within garnet of THO eclogites for which a mean date of  $1,831 \pm 5$  Ma has been interpreted to record peak metamorphism (Weller & St-Onge, 2017). A similar timing of *ca.* 1,860–1,820 Ma peak Trans-Hudson metamorphism resulting from collisional orogenesis has been interpreted from U-Pb zircon rim and monazite dates from the orogen in Baffin Island, Nunavut, Canada (Skipton et al., 2016). These geologic data strongly support that the Superior Province was conjoined with the Slave + Rae + Hearne provinces prior to 1,800 Ma in their present-day relative positions (Figure 1).

There are high-quality paleomagnetic poles for the Superior province during the time interval when the Manikewan Ocean was closing leading up to the Trans-Hudson orogeny (the *ca.* 1,880 Ma Molson dykes pole and the *ca.* 1,870 Ma Haig/Flaherty pole; Figure 9). There are no Paleoproterozoic paleomagnetic poles for the Superior Province during or after the Trans-Hudson orogeny that can test Laurentia's coherency with paleomagnetic data. The new  $1,779.1 \pm 2.3$  Ma ECMB paleomagnetic pole fills this gap.

While abundant paleomagnetic data have been developed from rocks within the THO (Symons & Harris, 2005), both the primary nature of the remanence directions as well as the age of remanence acquisition has been challenging to establish. As a result, relatively few poles from this interval during and following Laurentia's amalgamation have been included in curated pole compilations such as that compiled by the Nordic paleogeography workshops (Evans et al., 2021). The best constrained of these poles comes from the post-orogenic  $1,740 \pm 5$  Ma Cleaver Dykes of the Great Bear Magmatic Arc on the western margin of the Slave Province (Figure 1; Irving, 2004). The age of these dikes is constrained by a U-Pb baddeleyite date and there is a positive baked contact test supporting the interpretation that the pole is primary. As can be seen in Figure 6, the position of this *ca.* 1,740 Ma Cleaver Dykes pole for Laurentia (Irving, 2004) is similar to the new pole for the *ca.* 1,780 Ma ECMB diabase dikes (Figure 6). They do not share a common mean (as determined through Watson and bootstrap common mean tests; Tauxe et al., 2016), but are within  $11^\circ$  of one another (less when considering uncertainty). The similarity in these pole positions provides an independent test of the coherency of the Laurentia craton at that time.

An additional pole for comparison comes from hematite remanence of volcanics and sediments of the Baker Lake Group of the Dubawnt Supergroup which were deposited in a basin atop the suture between the Rae and Hearne provinces (Figures 1 and 6; Park et al., 1973). Both the depositional age of the succession and the age of hematite remanence are roughly constrained leading to a wide assigned age range of 1,820 to 1,750 Ma in Evans et al. (2021) for the pole. While the loose age constraints hinder firm comparisons, the broad similarity of this pole with the Cleaver Dykes pole of the Slave Province as well as that for Martin Formation ( $1,818 \pm 4$  Ma) and the Sparrow dikes ( $1,827 \pm 4$  Ma) of the Rae Province establishes a largely consistent position of the Churchill plate from *ca.* 1,820 to 1,740 Ma.

A less robust pole for comparison with the new ECMB pole comes from the post-orogenic Jan Lake Granite within the THO in southeast Saskatchewan developed in Gala et al. (1995). A U-Pb zircon date of  $1,758 \pm 1$  Ma for this granite was reported in Bickford et al. (2005). Directional data from the Jan Lake Granite falls into two groups. Based on thermal demagnetization behavior, Irving (2004) interpreted the "A" grouping to be a TRM held by magnetite that was acquired at the time of the emplacement of the intrusion *ca.* 1,758 Ma. The ECMB dikes pole shares a common mean with this Jan Lake Granite pole with overlapping  $A_{95}$  confidence circles (Figure 6). This result is consistent with both the Jan Lake Granite and ECMB being post-orogenic magmatic events that occurred following the amalgamation of Laurentia. This similarity suggests that despite the large uncertainty on the Jan Lake Granite pole and the ambiguity resulting from multiple directional groups that the pole does constrain the position of Laurentia *ca.* 1,758 Ma.

A pole that does not hold up to such comparative scrutiny is that developed for the Deschambault Pegmatites from within the THO (Figure 6c; Symons et al., 2000). This pole has been interpreted to constrain the position of Laurentia *ca.* 1,766 Ma—an age based on U-Pb monazite and allanite dates of other pegmatites in the region. As noted in D'Agrella-Filho et al. (2020), there are no field tests for this pole and the remanence directions from which it is calculated are quite close to the modern geomagnetic field. This pole was included in the curated Nordic paleogeography workshop compilation of Evans et al. (2021) less because of the quality of the individual pole, but rather because there are a number of poles of similar position to this one from the THO (Figure 6). Many of these poles have individual VGPs that are streaked between directions similar to the Jan Lake Granite and that of the present-local field. The direction of the Deschambault pole is far from the new *ca.* 1,780 Ma ECMB dikes pole. In contrast, the similarity of pole position between the new ECMB dikes pole and the *ca.* 1,758 Ma Jan Lake Granite pole as well as the *ca.* 1,740 Ma Cleaver Dykes pole supports that these poles, rather than the Deschambault Pegmatites pole, constrain Laurentia's position during this interval. This Deschambault Pegmatites pole played a role, in conjunction with other poles from the THO, such as that from the Wapisiu gneiss and the Deschambault Post pluton, in an interpretation that Laurentia's pole path was at a standstill in the vicinity of the Deschambault Pegmatites pole from *ca.* 1,800 Ma through to *ca.* 1,766 Ma (Symons et al., 2000; Symons & Harris, 2005). As reviewed in



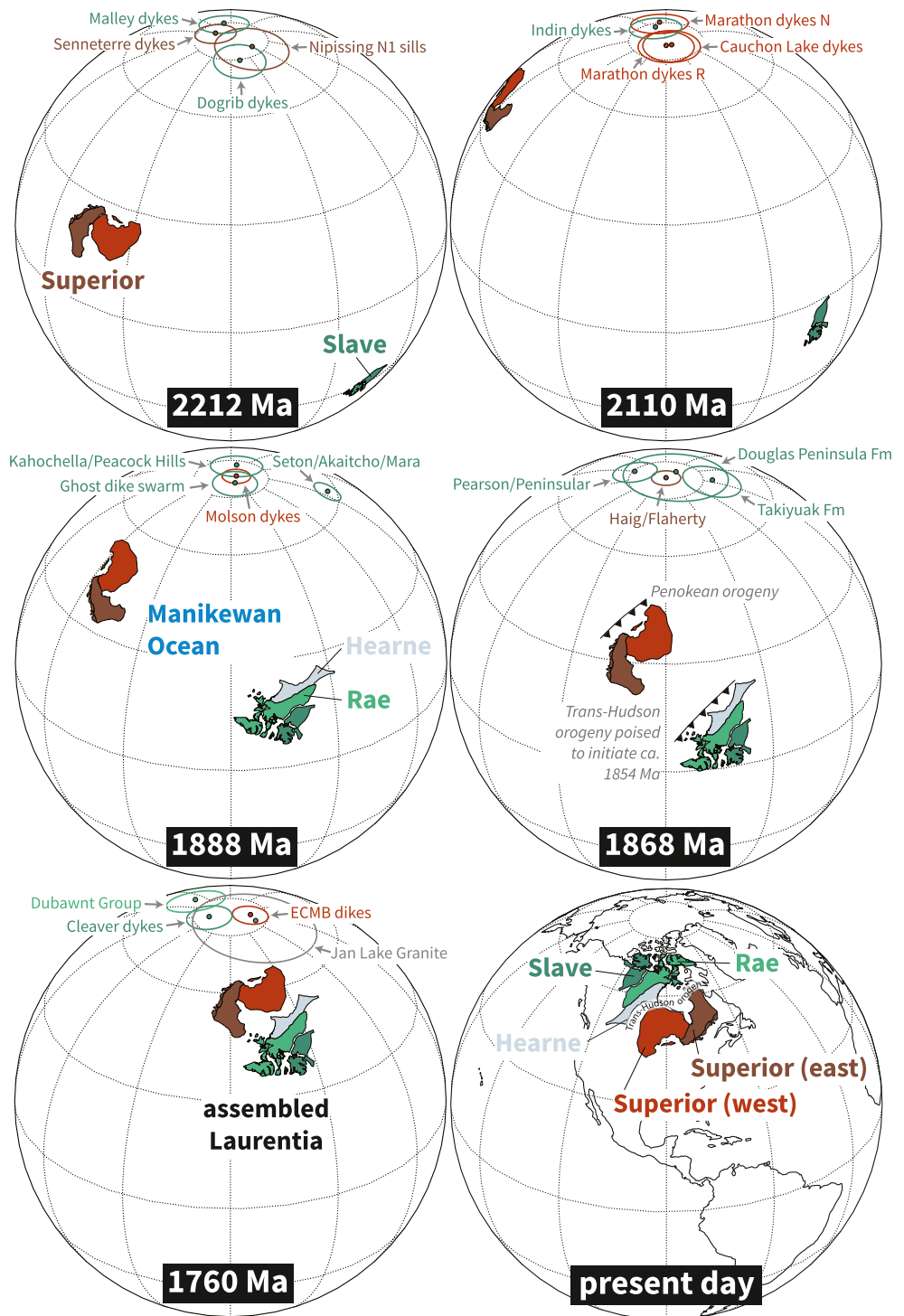


**Figure 9.** Paleogeographic reconstructions at five different times in the Paleoproterozoic and the position of the provinces at present. Paleomagnetic poles within 20 Myr of the given time (10 Myr for 1,888 and 1,868 Ma) are shown from the compilation of Evans et al. (2021) as well as the new East-Central Minnesota batholith (ECMB) pole. These data illustrate differential plate motion between the Superior and Slave Provinces that is required by the data leading up to the closure of the Manikewan-Hudson and the assembly of Laurentia during the Trans-Hudson orogeny. The ECMB pole is consistent with an assembled Laurentia following the Trans-Hudson orogeny which contrasts with the disparate orientations and paleolatitudes between Laurentia’s constituent provinces prior to the orogeny.

Raub (2008), there are numerous difficulties in interpreting these data from the Trans-Hudson orogen as useful constraints including: (1) a lack of field tests; (2) uncertainty in the timescale of cooling and the timing of the acquisition of magnetization in these slowly cooled units; (3) poorly constrained tilt corrections and (4) large secondary viscous remanent magnetizations that are prevalent due to the coarse grain-size of the igneous lithologies. The preferred interpretation of Raub (2008), which is echoed in D'Agrella-Filho et al. (2020), is that there is component mixing between primary directions (which would be in the vicinity of the Jan Lake Granite A Group pole and our new ECMB pole) and the present-day north pole as the result of unresolved viscous overprints (Figure 6). This component mixing leads to streaked site mean directions in individual studies as well as the database of Trans-Hudson orogen poles including the Deschambault Pegmatites pole (Figure 6; Raub, 2008). The new ECMB pole significantly strengthens this interpretation by demonstrating that a proposed northerly apparent polar wander path to satisfy the Deschambault Pegmatites pole and other Trans-Hudson orogen poles streaked between the Jan Lake Granite and the modern-day pole is indeed fictitious (Figure 6). Instead, the ECMB pole and the Cleaver Dykes pole establish the paleogeographic position of Laurentia to have been relatively consistent *ca.* 1,780–1,740 Ma (Figure 9).

### 6.3. The Paleogeography of Laurentia

As is expected by the geologic record of Trans-Hudson orogenesis, the similarity in pole positions from the southeastern margin of the Superior Provinces (the new ECMB pole) and the northwestern margin of the Slave Province (the Cleaver Dykes pole; Figure 6) indicate a coherent assembled Laurentia following 1.8 Ga (Figure 9). The coherency of the record of high-quality paleomagnetic poles at this time when the geologic record indicates a recently assembled Laurentia increases confidence that differing pole positions between Laurentia's Archean provinces earlier in the Paleoproterozoic are indeed a record of differential plate tectonic motion (Figure 9). There is a particularly rich record of paleomagnetic poles from the Archean Superior and Slave provinces that can be paired between 2.23 and 1.89 Ga that constrain the provinces to not be in their modern relative orientation and to be undergoing differential motion (Buchan et al., 2016; Mitchell et al., 2014; Swanson-Hysell, 2021). These poles result in reconstructions where prior to the Trans-Hudson orogeny there was an ocean basin between the Superior province and the Hearne + Rae + Slave provinces known as the Manikewan Ocean (Figure 9; Stauffer, 1984). The poles are consistent with the Superior Province approaching the joint Slave + Hearne + Rae provinces prior to the onset of the Trans-Hudson orogeny (Figure 9). These data provide strong evidence for mobile lid plate tectonics from 2.23 Ga onward (Buchan et al., 2016; Mitchell et al., 2014; Swanson-Hysell, 2021).

The orogenesis associated with Laurentia's assembly is hypothesized to have resulted in the formation of the supercontinent, or semi-supercontinent, Nuna (Hoffman, 1997; Evans et al., 2016; Evans & Mitchell, 2011). Given that Laurentia is the largest craton hypothesized to have been part of this supercontinent, its paleogeographic position is key to reconstructions of Nuna. The new ECMB pole provides higher confidence in the paleogeographic position of Laurentia in the time just following its formation from the collision of constituent Archean provinces (Figure 9). This new pole can be used to evaluate hypothesized connections between Laurentia and other cratons. There is an increasingly rich global database of paleomagnetic poles *ca.* 1,780 Ma including poles from the Amazonia, Baltica, India, Rio de la Plata, São Francisco and North China cratons (Bispo-Santos et al., 2014; D'Agrella-Filho et al., 2020; Shankar et al., 2018; Xu et al., 2014; Zhang et al., 2012).

One hypothesized connection of particular interest is that with Baltica. The two cratons have been hypothesized to have been conjoined such that they shared a margin with a long-lived history of accretionary orogenesis (Hoffman, 1997; Karlstrom et al., 2001). The proposed NENA configuration between Laurentia and Baltica allows for such a shared margin (Buchan et al., 2000; Evans & Pisarevsky, 2008; Gower et al., 1990). The increased concordance between *ca.* 1,780 and 1,750 paleomagnetic poles from Laurentia and Baltica upon the NENA rotation of Baltica can be seen in Figure 10. Paleomagnetic poles support a continued NENA connection until at least 1,260 Ma (supported by poles from Baltica's *ca.* 1,258 Ma post-Jotnian intrusions and Laurentia's *ca.* 1,267 Ma Mackenzie dikes) and perhaps to 1,120 Ma (where the paleomagnetic comparison is reliant on the *ca.* 1,122 Ma Salla dike of Baltica developed from a single cooling unit; Salminen et al., 2009). This connection supports the long-lived active margin where Laurentia grew through

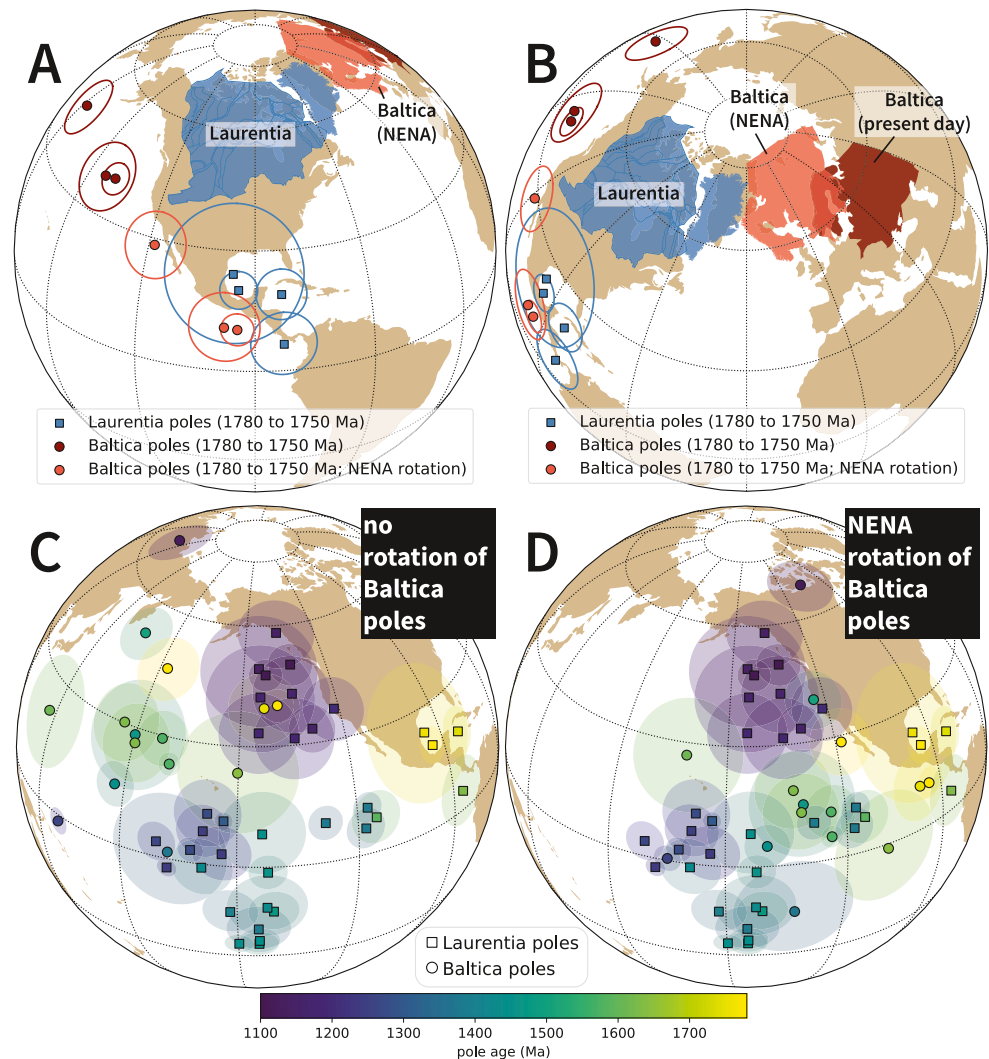


**Figure 10.** (a) Paleomagnetic poles for Laurentia and Baltica between 1,780 and 1,750 Ma with the Baltica poles shown with and without the NENA rotation (Euler pole for Baltica of  $[47.5^\circ, 001.5^\circ, +49.0^\circ]$  as in Evans and Pisarevsky, 2008). Baltica is shown in its present day location in dark red and shown in the NENA position in light red. (b) Same data as in panel A shown with a different center of projection which allows for easier visualization of the reconstructed position. (c and d) Comparison between poles between 1,780 and 1,110 Ma between Baltica and Laurentia without (c) and with (d) the NENA rotation. The poles that are shown are those from the Nordic compilation with “A” and “B” grades as well as the new East-Central Minnesota batholith (ECMB) pole from this study.

the rest of the Paleoproterozoic and through the Mesoproterozoic until the *ca.* 1.08 Ga continent-continent collision of the Grenvillian orogeny (Whitmeyer & Karlstrom, 2007).

## 7. Conclusions

The ECMB was emplaced following Penokean orogenesis on the southeast margin of the Superior Province. While the southeast margin of Laurentia experienced subsequent intervals of accretionary orogenesis, thermochronology data constrain the batholith to have a straight-forward history of post-emplacement rapid exhumation without substantial reheating. Subsequent orogenesis occurred well southeast of the batholith—consistent with the batholith having played a role in stabilizing Laurentian lithosphere. Comagmatic diabase dikes of the ECMB can be constrained through U-Pb geochronology on the felsic units to have been emplaced at  $1,779.1 \pm 2.3$  Ma. A new paleomagnetic pole developed from the magnetite remanence of these dikes provides a high-quality constraint on the position of Laurentia following Trans-Hudson orogenesis.

This pole confirms the coherency of an amalgamated Laurentia at the time and supports the NENA connection with Baltica. This paleomagnetic coherency further strengthens the case that previously disparate pole positions between the Superior and Slave provinces are the result of ca. 2.2–1.8 Ga mobile-lid plate tectonics. The geologic and paleomagnetic record of Laurentia is inconsistent with a stagnant-lid regime anytime over the past 2.2 billion years.

## Data Availability Statement

Paleomagnetic data associated with this study are available within the MagIC database (<https://www.earthref.org/MagIC/doi/10.1029/2021TC006751>;) and all data are within a Github repository associated with this work ([https://github.com/Swanson-Hysell-Group/2021\\_ECMB](https://github.com/Swanson-Hysell-Group/2021_ECMB)) that is also archived on Zenodo (<https://doi.org/10.5281/zenodo.4625041>). This repository also contains Python code related to calculations, visualizations and statistical tests discussed herein.

## Acknowledgments

This research was supported by the National Science Foundation through CAREER grant EAR-1847277 awarded to N.L.S.-H. Rock magnetic experiments using the MPMS were conducted at the Institute for Rock Magnetism which is supported by the Instrumentation and Facilities program of the National Science Foundation, Earth Science Division. The authors gratefully acknowledge Mark Schmitz and Jim Crowley for analytical support at the Boise State Isotope Geology Laboratory. Noah McLean provided insight for the methodology applied to interpret the uncertainty associated with the age of a unit bracketed by U-Pb dates. The authors thank Stearns County Parks for research permits that enabled sample collection in Quarry Park and Nature Preserve. The manuscript was improved through thoughtful reviews from Daniel Holm, Anthony Pivarunas, and an anonymous reviewer.

## References

- Ague, J. J. (1997). Thermodynamic calculation of emplacement pressures for batholithic rocks, California: Implications for the aluminum-in-hornblende barometer. *Geology*, 25(6), 563–566. [https://doi.org/10.1130/0091-7613\(1997\)025<0563:tcoepf>2.3.co;2](https://doi.org/10.1130/0091-7613(1997)025<0563:tcoepf>2.3.co;2)
- Besnus, M. J., & Meyer, A. J. (1964). Nouvelles données expérimentales sur le magnétisme de la pyrrhotine naturelle. *Proceedings of the International Conference on Magnetism*, 20, 507–511.
- Bickford, M. E., Mock, T. D., Steinhart, III, W. E., Collerson, K. D., & Lewry, J. F. (2005). Origin of the Archean Sask craton and its extent within the Trans-Hudson orogen: Evidence from Pb and Nd isotopic compositions of basement rocks and post-orogenic intrusions. *Canadian Journal of Earth Sciences*, 42, 659–684. <https://doi.org/10.1139/e04-064>
- Bispo-Santos, F., D'Agrella-Filho, M. S., Trindade, R. I. F., Janikian, L., & Reis, N. J. (2014). Was there SAMBA in Columbia? Paleomagnetic evidence from 1790 Ma Avanavero mafic sills (Northern Amazonian Craton). *Precambrian Research*, 244, 139–155. <https://doi.org/10.1016/j.precamres.2013.11.002>
- Boerboom, T. J., & Holm, D. K. (2000). *Paleoproterozoic intrusive igneous rocks of southeastern Stearns County, Central Minnesota*. Minnesota Geological Survey. Report of Investigations 56. Retrieved from <https://hdl.handle.net/11299/58796>
- Boerboom, T. J., Holm, D. K., & Van Schmus, R. (2005). *Granites of the East-Central Minnesota Batholith*. Minnesota Geological Survey Guidebook.
- Boerboom, T. J., Holm, D. K., & Van Schmus, R. (2011). Late Paleoproterozoic deformational, metamorphic, and magmatic history of east-central Minnesota. In *Archean to Anthropocene: Field guides to the geology of the mid-continent of North America* (pp. 1–23). Geological Society of America. <https://doi.org/10.1130/2011.0024>
- Boerboom, T. J., Setterholm, D. R., & Chandler, V. W. (1995). Bedrock geology pl. 2. In G. N. Meyer (Ed.), *Geologic atlas of Stearns county, Minnesota: Minnesota geological survey county atlas C-10, pt. A., 7 pls., scales 1:100,000 and 1:200,000*. Minnesota Geological Survey. Retrieved from <https://hdl.handle.net/11299/58515>
- Buchan, K. L., Mertanen, S., Park, R. G., Pesonen, L. J., Elming, S.-Å., Abrahamsen, N., & Bylund, G. (2000). Comparing the drift of Laurentia and Baltica in the Proterozoic: The importance of key palaeomagnetic poles. *Tectonophysics*, 319, 167–198. [https://doi.org/10.1016/S0040-1951\(00\)00032-9](https://doi.org/10.1016/S0040-1951(00)00032-9)
- Buchan, K. L., Mitchell, R. N., Bleeker, W., Hamilton, M. A., & LeCheminant, A. N. (2016). Paleomagnetism of ca. 2.13–2.11 Ga Indin and ca. 1.885 Ga Ghost dyke swarms of the Slave craton: Implications for the Slave craton APW path and relative drift of Slave, Superior and Siberian cratons in the Paleoproterozoic. *Precambrian Research*, 275, 151–175. <https://doi.org/10.1016/j.precamres.2016.01.012>
- Chamberlain, K. R., & Bowring, S. A. (2001). Apatite–feldspar U–Pb thermochronometer: A reliable, mid-range (~450°C), diffusion-controlled system. *Chemical Geology*, 172(1–2), 173–200. [https://doi.org/10.1016/S0009-2541\(00\)00242-4](https://doi.org/10.1016/S0009-2541(00)00242-4)
- Cherniak, D. J., Lanford, W. A., & Ryerson, F. J. (1991). Lead diffusion in apatite and zircon using ion implantation and Rutherford backscattering techniques. *Geochimica et Cosmochimica Acta*, 55(6), 1663–1673. [https://doi.org/10.1016/0016-7037\(91\)90137-t](https://doi.org/10.1016/0016-7037(91)90137-t)
- Cherniak, D. J., & Watson, E. B. (2001). Pb diffusion in zircon. *Chemical Geology*, 172(1–2), 5–24. [https://doi.org/10.1016/S0009-2541\(00\)00233-3](https://doi.org/10.1016/S0009-2541(00)00233-3)
- Cochrane, R., Spikings, R. A., Chew, D., Wotzlaw, J.-F., Chiaradia, M., Tyrrell, S., et al. (2014). High temperature (>350°C) thermochronology and mechanisms of Pb loss in apatite. *Geochimica et Cosmochimica Acta*, 127, 39–56. <https://doi.org/10.1016/j.gca.2013.11.028>
- Corrigan, D., Pehrsson, S., Wodicka, N., & de Kemp, E. (2009). The Palaeoproterozoic Trans-Hudson orogen: A prototype of modern accretionary processes. *Geological Society, London, Special Publications*, 327(1), 457–479. <https://doi.org/10.1144/sp327.19>
- D'Agrella-Filho, M. S., Teixeira, W., da Trindade, R. I., Patroni, O. A., & Prieto, R. F. (2020). Paleomagnetism of 1.79 Ga Pará de Minas mafic dykes: Testing a São Francisco/Congo-North China-Rio de la Plata connection in Columbia. *Precambrian Research*, 338, 105584. <https://doi.org/10.1016/j.precamres.2019.105584>
- Deenen, M. H. L., Langereis, C. G., van Hinsbergen, D. J. J., & Biggin, A. J. (2011). Geomagnetic secular variation and the statistics of palaeomagnetic directions. *Geophysical Journal International*, 186, 509–520. <https://doi.org/10.1111/j.1365-246X.2011.05050.x>
- Dewane, T. J., & Van Schmus, W. R. (2007). U–Pb geochronology of the Wolf River batholith, north-central Wisconsin: Evidence for successive magmatism between 1484 Ma and 1468 Ma. *Precambrian Research*, 157(1–4), 215–234. <https://doi.org/10.1016/j.precamres.2007.02.018>
- Dodson, M. H. (1973). Closure temperature in cooling geochronological and petrological systems. *Contributions to Mineralogy and Petrology*, 40(3), 259–274. <https://doi.org/10.1007/bf00373790>
- Evans, D. A. D., Li, Z. X., & Murphy, J. B. (2016). Four-dimensional context of Earth's supercontinents. In D. A. D. Evans, Z. X. Li, & J. B. Murphy (Eds.), *Supercontinent cycles through earth history* (pp. 1–14). Geological Society, London, Special Publications. <https://doi.org/10.1144/SP424.12>
- Evans, D. A. D., & Mitchell, R. N. (2011). Assembly and breakup of the core of Paleoproterozoic–Mesoproterozoic supercontinent Nuna. *Geology*, 39, 443–446. <https://doi.org/10.1130/G31654.1>

- Evans, D. A. D., Pesonen, L. J., Eglinton, B. M., Elming, S.-Å., Gong, Z., Li, Z.-X., et al. (2021). An expanding list of reliable paleomagnetic poles for Precambrian tectonic reconstructions. In L. J. Pesonen, D. A. D. Evans, S. Å. Elming, J. M. Salminen, & T. Veikkolainen (Eds.), *Ancient supercontinents and the paleogeography of the earth*. Elsevier.
- Evans, D. A. D., & Pisarevsky, S. A. (2008). Plate tectonics on early Earth? Weighing the paleomagnetic evidence. *Geological Society of America Special Paper*, 440, 249–263. [https://doi.org/10.1130/2008.2440\(1210.1130/2008.2440\(12\)\)](https://doi.org/10.1130/2008.2440(1210.1130/2008.2440(12)))
- Fairchild, L. M., Swanson-Hysell, N. L., Ramezani, J., Sprain, C. J., & Bowring, S. A. (2017). The end of midcontinent rift magmatism and the paleogeography of Laurentia. *Lithosphere*, 9(1), 117–133. <https://doi.org/10.1130/L580.1>
- Feinberg, J. M., Solheid, P. A., Swanson-Hysell, N. L., Jackson, M. J., & Bowles, J. A. (2015). Full vector low-temperature magnetic measurements of geologic materials. *Geochemistry, Geophysics, Geosystems*, 16, 301–314. <https://doi.org/10.1002/2014gc005591>
- Fisher, N. I., Lewis, T., & Embleton, B. J. J. (1987). *Statistical analysis of spherical data*. Cambridge University Press. <https://doi.org/10.1017/CBO9780511623059>
- Gala, M. G., Symons, D. T. A., & Palmer, H. C. (1995). Paleomagnetism of the Jan Lake granite, Trans-Hudson orogen. *Saskatchewan Geological Survey Summary of Investigations*, 95–4.
- Gower, C. F., Ryan, A. B., & Rivers, T. (1990). Mid-Proterozoic Laurentia-Baltica: An overview of its geological evolution and a summary of the contributions made by this volume. In C. F. Gower, T. Rivers, & A. B. Ryan (Eds.), *Mid-proterozoic Laurentia-Baltica*. Geological Association of Canada, Special Paper.
- Grove, M., & Harrison, T. M. (1996). 40Ar\* diffusion in Fe-rich biotite. *American Mineralogist*, 81, 940–951. <https://doi.org/10.2138/am-1996-7-816>
- Hanson, G. (1968). *K-Ar ages for hornblende from granites and gneisses and for basaltic intrusives in Minnesota*. Minnesota Geological Survey. Report of Investigations 8. Retrieved from <https://hdl.handle.net/11299/60191>
- Harrison, T. M. (1982). Diffusion of <sup>40</sup>Ar in hornblende. *Contributions to Mineralogy and Petrology*, 78(3), 324–331. <https://doi.org/10.1007/BF00398927>
- Hodgskiss, M. S. W., Dagnaud, O. M. J., Frost, J. L., Halverson, G. P., Schmitz, M. D., Swanson-Hysell, N. L., & Sperling, E. A. (2019). New insights on the Orosirian carbon cycle, early cyanobacteria, and the assembly of Laurentia from the Paleoproterozoic Belcher group. *Earth and Planetary Science Letters*, 520, 141–152. <https://doi.org/10.1016/j.epsl.2019.05.023>
- Hoffman, P. F. (1988). United plates of America, the birth of a craton: Early Proterozoic assembly and growth of Laurentia. *Annual Review of Earth and Planetary Sciences*, 16(1), 543–603. <https://doi.org/10.1146/annurev.ea.16.050188.002551>
- Hoffman, P. F. (1997). Tectonic genealogy of North America. In B. van der Pluijm, & S. Marshak (Eds.), *Earth structure: An introduction to structural geology and tectonics* (pp. 459–464). McGraw-Hill.
- Holm, D. K., Anderson, R., Boerboom, T. J., Cannon, W. F., Chandler, V., Jirsa, M., et al. (2007). Reinterpretation of Paleoproterozoic accretionary boundaries of the north-central United States based on a new aeromagnetic-geologic compilation. *Precambrian Research*, 157(1–4), 71–79. <https://doi.org/10.1016/j.precamres.2007.02.023>
- Holm, D. K., Darrah, K. S., & Lux, D. R. (1998). Evidence for widespread approximately 1760 Ma metamorphism and rapid crustal stabilization of the early Proterozoic (1870–1820 Ma) Penokean orogen, Minnesota. *American Journal of Science*, 298(1), 60–81. <https://doi.org/10.2475/ajs.298.1.60>
- Holm, D. K., & Lux, D. R. (1996). Core complex model proposed for gneiss dome development during collapse of the Paleoproterozoic Penokean orogen, Minnesota. *Geology*, 24(4), 343. [https://doi.org/10.1130/0091-7613\(1996\)024\(0343:ccmpfg\)2.3.co;2](https://doi.org/10.1130/0091-7613(1996)024(0343:ccmpfg)2.3.co;2)
- Holm, D. K., & Selverstone, J. (1990). Rapid growth and strain rates inferred from synkinematic garnets, Penokean orogeny, Minnesota. *Geology*, 18(2), 166–169. [https://doi.org/10.1130/0091-7613\(1990\)018\(0166:rgasri\)2.3.co;2](https://doi.org/10.1130/0091-7613(1990)018(0166:rgasri)2.3.co;2)
- Holm, D. K., Van Schmus, W. R., MacNeill, L. C., Boerboom, T. J., Schweitzer, D., & Schneider, D. (2005). U-Pb zircon geochronology of Paleoproterozoic plutons from the northern midcontinent, USA: Evidence for subduction flip and continued convergence after geon 18 Penokean orogenesis. *Geological Society of America Bulletin*, 117(3), 259–275. <https://doi.org/10.1130/b25395.1>
- Holm, D., Medaris, L. G., McDannell, K. T., Schneider, D. A., Schulz, K., Singer, B. S., & Jicha, B. R. (2019). Growth, overprinting, and stabilization of Proterozoic Provinces in the southern Lake Superior region. *Precambrian Research*, 339, 105587. <https://doi.org/10.1016/j.precamres.2019.105587>
- Holm, D., Schneider, D., & Coath, C. D. (1998). Age and deformation of Early Proterozoic quartzites in the southern Lake Superior region: Implications for extent of foreland deformation during final assembly of Laurentia. *Geology*, 26(10), 907–910. [https://doi.org/10.1130/0091-7613\(1998\)026\(0907:aadoep\)2.3.co;2](https://doi.org/10.1130/0091-7613(1998)026(0907:aadoep)2.3.co;2)
- Horan, M. F., Hanson, G. N., & Spencer, K. J. (1987). Pb and Nd isotope and trace element constraints on the origin of basic rocks in an early Proterozoic igneous complex, Minnesota. *Precambrian Research*, 37(4), 323–342. [https://doi.org/10.1016/0301-9268\(87\)90081-7](https://doi.org/10.1016/0301-9268(87)90081-7)
- Irving, E. (2004). Early Proterozoic geomagnetic field in western Laurentia: Implications for paleolatitudes, local rotations and stratigraphy. *Precambrian Research*, 129(3–4), 251–270. <https://doi.org/10.1016/j.precamres.2003.10.002>
- Jirsa, M., Boerboom, T., & Chandler, V. (2012). *S-22, geologic map of Minnesota, Precambrian bedrock geology (Tech. Rep)*. Minnesota Geological Survey. Retrieved from <https://hdl.handle.net/11299/154540>
- Karlstrom, K. E., Ahall, K.-I., Harlan, S. S., Williams, M. L., McLelland, J., & Geissman, J. W. (2001). Long-lived (1.8–1.0 Ga) convergent orogen in southern Laurentia, its extensions to Australia and Baltica, and implications for refining Rodinia. *Precambrian Research*, 111(1–4), 5–30. [https://doi.org/10.1016/S0301-9268\(01\)00154-1](https://doi.org/10.1016/S0301-9268(01)00154-1)
- Kissin, S. A., & Scott, S. D. (1982). Phase relations involving pyrrhotite below 350 degrees C. *Economic Geology*, 77(7), 1739–1754. <https://doi.org/10.2113/gsecongeo.77.7.1739>
- Ludwig, K. R. (1998). On the treatment of concordant uranium-lead ages. *Geochimica et Cosmochimica Acta*, 62, 665–676. [https://doi.org/10.1016/s0016-7037\(98\)00059-3](https://doi.org/10.1016/s0016-7037(98)00059-3)
- Medaris, L. G., Singer, B. S., Jicha, B. R., Malone, D. H., Schwartz, J. J., Stewart, E. K., et al. (2021). Early Mesoproterozoic evolution of midcontinental Laurentia: Defining the geon 14 Baraboo orogeny. *Geoscience Frontiers*, 12(5), 101174. <https://doi.org/10.1016/j.gsf.2021.101174>
- Meert, J. G., Pivarunas, A. F., Evans, D. A. D., Pisarevsky, S. A., Pesonen, L. J., Li, Z.-X., et al. (2020). The magnificent seven: A proposal for modest revision of the quality index. *Tectonophysics*, 790, 228549. <https://doi.org/10.1016/j.tecto.2020.228549>
- Mitchell, R. N., Bleeker, W., van Breemen, O., Lecheminant, T. N., Peng, P., Nilsson, M. K. M., & Evans, D. A. D. (2014). Plate tectonics before 2.0 Ga: Evidence from paleomagnetism of cratons within supercontinent Nuna. *American Journal of Science*, 314(4), 878–894. <https://doi.org/10.2475/04.2014.03>
- Mutch, E. J. F., Blundy, J. D., Tattitch, B. C., Cooper, F. J., & Brooker, R. A. (2016). An experimental study of amphibole stability in low-pressure granitic magmas and a revised Al-in-hornblende geobarometer. *Contributions to Mineralogy and Petrology*, 171(10). <https://doi.org/10.1007/s00410-016-1298-9>

- Park, J. K., Irving, E., & Donaldson, J. A. (1973). Paleomagnetism of the Precambrian Dubawnt Group. *Geological Society of America Bulletin*, 84(3), 859–870. [https://doi.org/10.1130/0016-7606\(1973\)84\(859:potpdg\)2.0.co;2](https://doi.org/10.1130/0016-7606(1973)84(859:potpdg)2.0.co;2)
- Pehrsson, S. J., Eglinton, B. M., Evans, D. A. D., Huston, D., & Reddy, S. M. (2015). Metallogeny and its link to orogenic style during the Nuna supercontinent cycle. *Geological Society, London, Special Publications*, 424, 83–94. <https://doi.org/10.1144/SP424.5>
- Raub, T. M. (2008). *Paleomagnetism of Dubawnt Supergroup, Baker Lake basin, Nunavut, Canada: Refining Laurentia's paleoproterozoic apparent polar wander path (Unpublished doctoral dissertation)*. Yale University.
- Rothstein, D. A., & Manning, C. E. (2003). Geothermal gradients in continental magmatic arcs: constraints from the eastern Peninsular Ranges Batholith, Baja California, Mexico. In *Baja California, Mexico. Tectonic evolution of northwestern Mexico and the Southwestern USA* (p. 374). Geological Society of America Special Paper. <https://doi.org/10.1130/0-8137-2374-4.337>
- Salminen, J., Pesonen, L. J., Mertanen, S., Vuollo, J., & Airo, M.-L. (2009). Palaeomagnetism of the Salla Diabase Dyke, northeastern Finland, and its implication for the Baltica-Laurentia entity during the Mesoproterozoic. *Geological Society, London, Special Publications*, 323(1), 199–217. <https://doi.org/10.1144/SP323.9>
- Schmitz, M. D., Southwick, D. L., Bickford, M. E., Mueller, P. A., & Samson, S. D. (2018). Neoproterozoic and Paleoproterozoic events in the Minnesota River Valley subprovince, with implications for southern Superior craton evolution and correlation. *Precambrian Research*, 316, 206–226. <https://doi.org/10.1016/j.precamres.2018.08.010>
- Schoene, B., & Bowering, S. A. (2007). Determining accurate temperature-time paths from U-Pb thermochronology: An example from the Kaapvaal craton, southern Africa. *Geochimica et Cosmochimica Acta*, 71(1), 165–185. <https://doi.org/10.1016/j.gca.2006.08.029>
- Schulz, K. J., & Cannon, W. F. (2007). The Penokean orogeny in the Lake Superior region. *Precambrian Research*, 157(1–4), 4–25. <https://doi.org/10.1016/j.precamres.2007.02.022>
- Shankar, R., Srinivasa Sarma, D., Ramesh Babu, N., & Parashuramulu, V. (2018). Paleomagnetic study of 1765 Ma dyke swarm from the Singhbhum Craton: Implications to the paleogeography of India. *Journal of Asian Earth Sciences*, 157, 235–244. <https://doi.org/10.1016/j.jseas.2017.08.026>
- Skipton, D. R., St-Onge, M. R., Schneider, D. A., & McFarlane, C. R. M. (2016). Tectonothermal evolution of the middle crust in the Trans-Hudson orogen, Baffin Island, Canada: Evidence from petrology and monazite geochronology of sillimanite-bearing migmatites. *Journal of Petrology*, 57(8), 1437–1462. <https://doi.org/10.1093/petrology/egw046>
- Smye, A. J., Marsh, J. H., Vermeesch, P., Garber, J. M., & Stockli, D. F. (2018). Applications and limitations of U-Pb thermochronology to middle and lower crustal thermal histories. *Chemical Geology*, 494, 1–18. <https://doi.org/10.1016/j.chemgeo.2018.07.003>
- Southwick, D. L., Morey, G. B., & Mossler, J. H. (1986). Fluvial origin of the lower Proterozoic Sioux Quartzite, southwestern Minnesota. *Geological Society of America Bulletin*, 97(12), 1432–1441. [https://doi.org/10.1130/0016-7606\(1986\)97\(1432:FOOTLP\)2.0.CO;2](https://doi.org/10.1130/0016-7606(1986)97(1432:FOOTLP)2.0.CO;2)
- Stauffer, M. R. (1984). Manikewan: An early Proterozoic ocean in central Canada, its igneous history and orogenic closure. *Precambrian Research*, 25(1), 257–281. [https://doi.org/10.1016/0301-9268\(84\)90036-6](https://doi.org/10.1016/0301-9268(84)90036-6)
- Swanson-Hysell, N. L. (2021). The Precambrian paleogeography of Laurentia. In L. J. Pesonen, D. A. D. Evans, S. Å. Elming, J. M. Salminen, & T. Veikkolainen (Eds.), *Ancient supercontinents and the paleogeography of the earth*. Elsevier.
- Swanson-Hysell, N. L., Hoaglund, S. A., Crowley, J. L., Schmitz, M. D., Zhang, Y., & Miller, J. D. (2020). Rapid emplacement of massive Duluth complex intrusions within the North American Midcontinent Rift. *Geology*, 49, 185–189. <https://doi.org/10.1130/g47873.1>
- Swanson-Hysell, N. L., Ramezani, J., Fairchild, L. M., & Rose, I. R. (2019). Failed rifting and fast drifting: Midcontinent Rift development, Laurentia's rapid motion and the driver of Grenvillian orogenesis. *Geological Society of America Bulletin*, 131, 913–940. <https://doi.org/10.1130/b31944.1>
- Symons, D. T. A., & Harris, M. J. (2005). Accretion history of the Trans-Hudson orogen in Manitoba and Saskatchewan from paleomagnetism. *Canadian Journal of Earth Sciences*, 42(4), 723–740. <https://doi.org/10.1139/e04-090>
- Symons, D. T. A., Symons, T. B., & Lewchuk, M. T. (2000). Paleomagnetism of the Deschambault pegmatites: Stillstand and hairpin at the end of the paleoproterozoic Trans-Hudson orogeny, Canada. *Physics and Chemistry of the Earth-Part A: Solid Earth and Geodesy*, 25(5), 479–487. [https://doi.org/10.1016/s1464-1895\(00\)00074-0](https://doi.org/10.1016/s1464-1895(00)00074-0)
- Tauxe, L., Shaar, R., Jonestrask, L., Swanson-Hysell, N. L., Minnett, R., Koppers, A. A. P., et al. (2016). PmagPy: Software package for paleomagnetic data analysis and a bridge to the magnetism information consortium (MagIC) database. *Geochemistry, Geophysics, Geosystems*, 17, 2450–2463. <https://doi.org/10.1002/2016GC006307>
- Thébault, E., Finlay, C. C., Beggan, C. D., Alken, P., Aubert, J., Barrois, O., et al. (2015). International geomagnetic reference field: The 12th generation. *Earth Planets and Space*, 67(1), 79. <https://doi.org/10.1186/s40623-015-0228-9>
- Van der Voo, R. (1990). The reliability of paleomagnetic data. *Tectonophysics*, 184(1), 1–9. [https://doi.org/10.1016/0040-1951\(90\)90116-P](https://doi.org/10.1016/0040-1951(90)90116-P)
- Vermeesch, P. (2018). IsoplotR: A free and open toolbox for geochronology. *Geoscience Frontiers*, 9(5), 1479–1493. <https://doi.org/10.1016/j.gsf.2018.04.001>
- Verwey, E. J. W. (1939). Electronic conduction of magnetite (Fe<sub>3</sub>O<sub>4</sub>) and its transition point at low temperatures. *Nature*, 144, 327–328. <https://doi.org/10.1038/144327b0>
- Weller, O. M., & St-Onge, M. R. (2017). Record of modern-style plate tectonics in the Palaeoproterozoic Trans-Hudson orogen. *Nature Geoscience*, 10, 305–311. <https://doi.org/10.1038/ngeo2904>
- Whitmeyer, S., & Karlstrom, K. (2007). Tectonic model for the Proterozoic growth of North America. *Geosphere*, 3(4), 220–259. <https://doi.org/10.1130/GES00055.1>
- Xu, H., Yang, Z., Peng, P., Meert, J. G., & Zhu, R. (2014). Paleo-position of the North China craton within the supercontinent Columbia: Constraints from new paleomagnetic results. *Precambrian Research*, 255, 276–293. <https://doi.org/10.1016/j.precamres.2014.10.004>
- Zhang, S., Li, Z.-X., Evans, D. A. D., Wu, H., Li, H., & Dong, J. (2012). Pre-Rodinia supercontinent Nuna shaping up: A global synthesis with new paleomagnetic results from North China. *Earth and Planetary Science Letters*, 353–354, 145–155. <https://doi.org/10.1016/j.epsl.2012.07.034>